Budker Institute of Nuclear Physics

B. F. Bayanov, V. P. Belov, E. D. Bender, M. V. Bokhovko,
G. I. Dimov, V. N. Kononov, O. E. Kononov, N. K. Kuksanov,
V. E. Palchikov, V. A. Pivovarov, R. A. Salimov, G. I. Silvestrov,
A. N. Skrinsky, N. A. Solovieva, S. Yu. Taskaev

Accelerator based neutron source for the neutron-capture and fast neutron therapy at hospital

(Physical project)

Budker INP 97-89

Novosibirsk

1997

Accelerator based neutron source for the neutron-capture and fast neutron therapy at hospital

B. F. Bayanov[1], V. P. Belov[1], E. D. Bender[1], M. V. Bokhovko[2], G. I. Dimov[1], V. N. Kononov[2], O. E. Kononov[2], N. K. Kuksanov[1], V. E. Palchikov[1], V. A. Pivovarov[2], R. A. Salimov[1], G. I. Silvestrov[1], A. N. Skrinsky[1], N. A. Solovieva[2], S. Yu. Taskaev[1]

Abstract

Discussed is the proton accelerator complex for neutron production in lithium target, which can operate in two modes. The first provides neutron beam with good forward direction in 25° in energy range of 15÷30 keV, directly applicable for neutron-capture therapy with high efficiency of proton beam use. The proton energy in this mode is 1.883 ÷ 1.890 MeV that is near the threshold of ^{7}Li(p,n)^{7}Be reaction. In the second mode, at proton energy of 2.5 MeV, the complex produced neutron beam with spectrum maximum at 790 keV which can be used directly for fast neutron therapy and for neutron-capture therapy after moderation.

The project of such neutron source is based on the 2.5 MeV original electrostatic accelerator tandem with vacuum insulation developed at BINP which is supplied with high voltage rectifier. The rectifier is produced in BINP as a part of ELV-type industrial accelerator. Design features of tandem determining its high reliability in operation with high current (up to 40 mA) H^- ion beam are discussed. They are: the absence of ceramic accelerator columns around the beam passage region, good conditions for pumping out of charge-exchange gaseous target region, strong focusing optics and high acceleration rate minimizing the space charge effects. The possibility of stabilization of protons energy with accuracy level of 0.1 % necessary for operation in the near threshold region is considered. The design description of H^- continuous ion source with current 40 mA is also performed.

For operation with 100 kW proton beam it is proposed to use liquid lithium targets. A thin lithium layer on the surface of tungsten disk cooled intensively by liquid metal heat carrier is proposed for use in case of vertical beam, and a flat liquid lithium jet flowing through the narrow nozzle — for horizontal beam.

---

[1] Budker Institute of Nuclear Physics, Novosibirsk, Russia

[2] Physics-Energy Institute named by A.I. Leipunsky, Obninsk, Russia

Contents

1 Conception of the accelerator based neutron source for the neutron-capture and fast neutron therapy at hospitals

Introduction

At present, the beam therapy is one the basic method for curing malignant tumors. Recently, the ever increasing attention in therapy was drawn to the use of neutron beams. Quite confident evidences of the successful use of neutrons in both the beam and combined therapy of tumors were obtained in the USA, Japan, Germany, Russia, Great Britain, France.

The neutron therapy, i.e. the irradiation of malignant tumor by the neutron flux is presently realized in two versions: a neutron-capture therapy (NCT) and fast neutron therapy (FNT).

• NCT, whose idea was proposed in 1936 (in 4 years after the neutron discovery) [1], consists in that the isotope with a large absorption cross-section of thermal neutron is introduced into the patient body mainly through its blood. At present, the mostly studied and frequently used in clinic practice is the version of the boron neutron capture therapy (BNCT) [2,3]. The boron containing compounds enriched in the isotope ^{10}B are synthesized. This compound introduced into the patient blood produce in the tumor cell the ^{10}B isotope concentration 30 $\mu g/g$ while in surrounding normal tissue cell to be ~ 10 $\mu g/g$. In neutron reaction $^{10}B(n,\alpha)^{7}Li$ the charged particles are produced with the total kinetic energy ~ 2.4 MeV and with a range in a tissue ~ 10 μm i.e. of the order of the size of a man's tumor cell. As a result, the cell comprising ^{10}B is effectively destroyed. Because of higher concentration of ^{10}B-isotope in the tumor cells mainly the cancer cell are destroyed. Thus, the basic idea of BNCT is that a neutron "finds" out the tumor cells and destroys them.

At the same time, some other versions of NCT are presently considered with the use other isotopes with high neutrons absorbtion ^{6}Li and ^{155,157}Gd [4].

The main requirements to the neutron beam for NCT are given in the following way:

1. Neutron energy should mainly be ranged from 1 *eV* to a few tens *keV*. This region is related to that usually the cancer tumor is located under the normal tissue at a depth of 30÷70 *mm*. The thermal neutrons (the most intensively absorbed with ^{10}B penetrate weakly the tissue and produce the major load on the surface layers (primarily on the skin) with no desirable effect in the deep tumor. Epithermal neutrons passing through the normal tissue layers are thermalized resulting in the peak of the thermal neutron flux in the deep tissue and thus providing the maximum of absorbed doze in the irradiated tumor. At the same time, there should have no fast neutrons and the spectrum upper boundary should not exceed a few ten *keV*. This is related to the fact that fast neutrons produce the main radiation effect in the tissue due to the recoiling protons has its maximum on the surface tissues and has no selective character.

2. The required intensity of a neutron beam is determined by the required absorbed radiation dose in single treatment and by the desirable exposition duration. The estimates show that at a 10 *min* exposition, for attaining an absorbed dose in a tumor with the ^{10}B concentration of 30 $\mu g/g$ is 20 *Gy* the epithermal neutron flux is required to be $(0.5\div1)\times10^{10}$ $cm^{-2}s^{-1}$. It is evident that the neutron flux value can be reduced at the same absorbed dose either by the extension of irradiation time or by an increase in ^{10}B concentration in tumor.

3. It is desirable that the absorbed dose produced by fast neutrons and by accompanying gamma-rays should not exceed 10 % of the therapeutical dose, i.e. 2 *Gy*.

4. The neutron beam should be well-collimated, i.e. with a slight divergener and quite distinct boundaries.

• The fast neutron therapy uses the fast neutron beams with high penetrability in tissue. The main therapeutical effect is achieved due to recoiling protons and heavier recoiling nuclei. The work performed at the Medical Radiological Center (MRRC RAMS) in collaboration with GSI Institute of Physics and Power Engineering (IPPE) in Obninsk [5] has shown the promising results in the use of a beam of fast neutrons from the BR-10 reactor in curing the old radiorestant tumors. Beginning from 1985, MRRC has conducted the successful cure of 230

patients with malignant tumors of the head, neck, dairy gland, osteogeneous sarcomas with the neutron beam B-3 from the BR-10 reactor. The main requirements to the fast neutron beam for FNT are in the following:

1. The neutron spectrum should be similar to the neutron spectrum of uranium fission. A fraction of neutrons with an energy over 100 keV in the beam spectrum should be 90 %.
2. The neutron flux on the collimator output should be ~ 1×10^{9} $cm^{-2}s^{-1}$.
3. The dose produced by an accompanying gamma radiation can be 50 % of the total dose.

1.1 Neutron sources for NCT and FNT

The nuclear reactor is the most powerful stationary source of neutrons. At a 1 MW heat power in reactor, ~ 10^{17} neutrons per second are produced. It is quite natural that the beams of reactor neutrons have been used for the NCT and FNT purposes. At present, in the world there are a few active operating therapeutical beams on the nuclear reactors of various kinds and powers [6]. In addition, the detailed projects are published for various therapeutical facilities which to a great extent take into account the medical and radiological requirements to neutron beams [7-9].

Since the neutron spectrum of the reactor core does not satisfy the NCT requirements because of a substantial fraction of fission neutrons, for producing a beam with the required parameters the special filters are used. For this purpose, the most frequently used is the composition of the heavy water and aluminum or its oxide in proportion 1:10 with a length of 1 m.

For the attenuation of gamma-rays the 10 cm thick Pb or Bi layers are used and thermal neutrons are absorbed by Cd or Li. Such filters can conditionally be called as scattering filters. The required neutron spectrum is achieved as a result of multiple scattering in a quite length medium moderating neutrons to epithermal energy. On the output of such a filter, a 1 m thick collimator should be installed to form the beam of required geometric dimensions. Such a structure of a neutron beam formation for NCT leads to that for providing the necessary beam intensity with the required spectral characteristics one has to get quite high neutron flux in the reactor core and as a consequence, its average power density in core and substantial power of reactor. For example, the MTR reactor designed for medical research has a power of 10 MW.

Some other reactors developed as sources of neutrons for NCT have a power ranging from 5 to 20 *MW*.

Another approach for the formation of neutron spectrum required for NCT [9] is the use of special filter made of material with large neutron cross-section at an energy of neutrons above ~ 10 *keV* and a small neutron cross-section in the range of epithermal neutrons. A ^{64}Ni isotope can be served as an example of such a filter. This filter is transmission operated filter removing from a beam the neutrons with energies over 10 *keV* and enabling the passage of useful for NCT epithermal neutrons. The use of transmission filter enables one to achieve the required beam parameters as, for example, in the use of fluid fuel reactor of 200 *kW* in power [9].

The main characteristics of the reactor neutron beams for NCT are given in Table 1.

Table 1.

Reactor	Power, *MW*	Filter	F_{epith}, $cm^{-2}c^{-1}$	Treatment time, *min*
MTR (INEL)	10	Al/D_2O/Li	1.7×10^{10}	10
MIT R-II (MIT)	5	Al/D_2O/Li	4×10^{9}	40
BMRR (BNL)	3	Al/D_2O/Li	1.8×10^{9}	90
Solution (PEI)	0.2	^{64}Ni/Al/S	2.8×10^{9}	60

In Obninsk over 10 years the studies of the fast neutron therapy have been conducted within the frame of collaboration between two research centers: SRC RF IPPE having the fast neutron reactor BR-10 at a power of 6 *MW* with the sodium coolant carrier and RIRC RAMS where the methods of beam therapy are developed and the complex cure of cancer tumors is performed. The FNT is realized on the horizontal neutron beam of the B-3 reactor with maximum sizes of 10×10 cm^2. The neutron spectrum is broad enough with mean energy of 0.8 *MeV*. The density of the fast neutron flux is 3×10^8 $cm^{-2}s^{-1}$. The typical duration of exposure is 10÷20 *min*. The fluid fuel reactor whose project was developed at IPPE enables one to get the fast neutron beam for FNT with a flux density of up to 2.5×10^{10} $cm^{-2}s^{-1}$.

In conclusion of the brief description of neutron beam characteristics for FNT and NCT based on nuclear reactors let us note some of their advantages and disadvantages:

1. Although the existing beams for NCT do not provide the necessary flux density and require large expositions (≥ 60 *min*), the neutron beams of designed special medical reactors satisfy the basic requirements to NCT and FNT in their spectral characteristics and exposure duration (≥ 10 *min*).

2. The nuclear reactor in its stationary regime of operation has the constant power level and the beam composition thereby providing standard expositions.

The following factors can be considered as the serious disadvantages of reactor therapeutical facilities:

1. A powerful reactor is very complex and expensive facility whose maintenance put quit strong requirements to nuclear safety.

2. With quite a rare exception, the cancer therapy centers and clinics are usually remote from the physics centers having nuclear reactors.

These circumstances led to that in recent years, the problems of the development of a neutron source for NCT based on the compact and inexpensive accelerator which can used for every cancer clinic are the subject of intense discussions.

At present, various versions of neutron sources for NCT using the cheap accelerators of direct action are conceptually developed [10,11]. For obtaining neutrons the nuclear reactors on light nuclei such as $T(p, n)^3He$, $^7Li(p, n)^7Be$, $^9Be(p, n)^9B$ and other are used. For obtaining neutrons in these reactions is need to have the protons up to $2 \div 2.5$ *MeV*.

The problems of the development of an intense accelerator-based neutron source for NCT are regularly discussed on the biannual International Symposia on the neutron capture therapy of cancer, on the International Conferences on the applications of accelerators in science and technology. In 1994, in Jackson (USA), the 1st International Workshop "Accelerator-Based Neutron Sources for BNCT" has been held [12]. On these meetings, several projects of high current compact accelerators applicable to the development of neutron sources for NCT have been presented.

1.2 Parameters of neutron source based on the reaction ^{7}Li(p,n)^{7}Be

The reaction ^{7}Li(p,n)^{7}Be is widely used for obtaining monoenergetic neutrons in the nuclear physics experiments and it is quite well studied [13]. This reaction is the threshold reaction. The reaction energy is Q = -1.644 MeV and the threshold value of proton energy is E = 1.881 MeV.

Near-threshold Region

There is a broad resonance with J = 2 near the threshold. Because of this resonance, the reaction cross-section increases sharply over the threshold value and it has foot-step form. The neutrons escaping the reaction near the threshold have an orbital momentum l = 0 and, consequently, an isotopic angular distribution in the center-mass system (CMS). These two important circumstances enable the description of the spatial-energy distribution of escaping neutrons in the laboratory system (LS) with the help of analytic expressions [14]. Using a simple approximation of homogeneous stopping of protons in lithium due to ionization losses these analytic expressions have the form:

$$Y_{\pm} = 3\times10^{3}\sqrt{E_p - 1881}\left(1+6\sqrt{\frac{E_p-1881}{E_p}}\right)^{-2}\frac{\alpha\left(Z\pm\cos\psi\right)}{Z\cos\psi\pm\left(49-\sin^2\psi\right)},$$

where $Y_{\pm} = d^2n/dE_n d\omega$ [$neutron/(eV\ sr\ \mu C)$] — is a doubly differential yield (DDY) of neutrons per the unit of their energies per the unit of solid angle and per 1 μC of protons; ψ is an escaping angle of neutrons in LS with respect to the direction of proton beam; E_p is an energy of protons [keV], Z and α are dimensionless parameters determined by the following relations:

$$Z^2 = \alpha^{-2} - \sin^2\psi,$$

$$\alpha^2 = M_p M_n E_p\left[M_{Be}M_{Li}\left(E_p - 1881\right)\right]^{-1},$$

comprising masses of interacting particles. An energy of neutron in LS determined by the following relation:

$$E_{n\pm} = \frac{M_n M_p}{\left(M_{Be}+M_n\right)^2}E_p\left(Z\pm\cos\psi\right)^2.$$

Signs "+" and "-" evidence the double character of energy value for neutrons and DDY at $\alpha > 1$ which correspond to neutrons escaping CMS into the front and back hemispheres, respectively.

The relations given enable one within the frame of declared approximations to calculate an energy distribution and an absolute yield of neutrons from a thick metal lithium target. The relations are valid up to the proton energy level of ~ 1920 *keV* which corresponds to $\alpha = 1$.

Fig.1 shows the doubly differentiated yield of neutrons from a thick metal lithium target and an angular distribution of escaping neutrons in LS in the polar coordinates at an initial proton energy of 1886 *keV*.

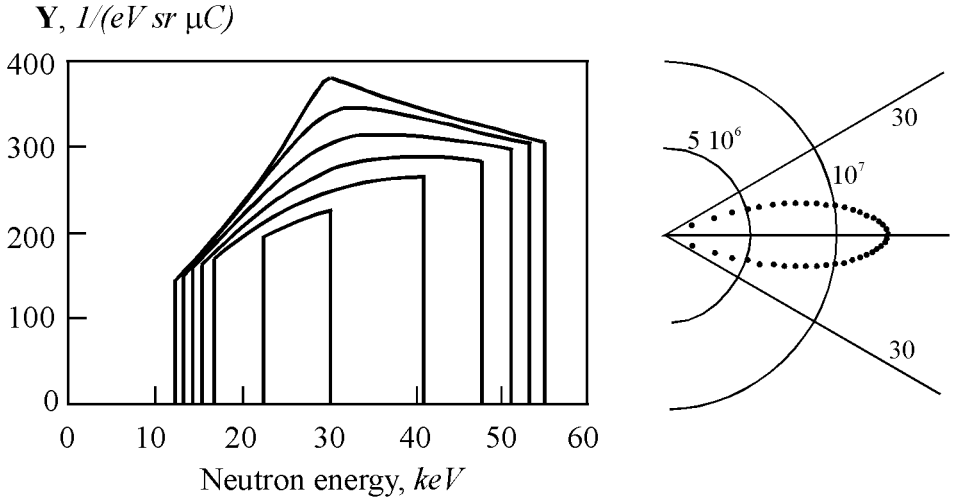

Figure 1: The doubly differential yield of neutrons from thick metallic lithium target for various laboratory escape angle (angle step is 5°) and angular distribution of neutrons in polar coordinates at an initial proton energy of 1886 keV.

Not the important for NCT features of the neutron source based on the use of the reaction ^{7}Li(p,n)^{7}Be in the near-threshold region.

1. The source has a well district direction ahead related to the specificity of kinematics of the threshold nuclear reactions (so-called the "kinematics collimation").

2. The spectrum of neutrons lies in the energy region 15 ÷ 50 *keV* acceptable for NCT and it has the distinct upper boundary determined by physics conditions with no "tail" of fast neutrons.

There circumstances enable one to consider the possibility of using such a source for the irradiation in the open geometry at a short distance between the source and subject with no use of an external collimator.

Table 2 shows the calculated value of the total yield of neutrons from $^{7}Li(p,n)^{7}Be$ reaction and limit escaping angle in the near-threshold region.

Table 2.

Proton energy, *keV*	Total yield neutrons at 10 *mA*, s^{1}	Limit angle of escape, *grad*	Limit energy of neutrons, *keV*
1883	8.47×10^{9}	13.2	44.8
1884	1.46×10^{10}	16.1	48.7
1885	2.15×10^{10}	18.6	52
1886	2.91×10^{10}	21	55.1
1891	7.11×10^{10}	30.9	67.9
1896	1.18×10^{11}	38.2	78.6
1901	1.67×10^{11}	45.4	88.3
1911	2.71×10^{11}	60.5	105.9
1920	3.66×10^{11}	81.7	120.6

Since for the use in NCT quite broad neutron beams are required which are determined by the tumor sizes, it is reasonable to use the targets of ~ 5 *cm* in diameter. In this case, the problem of reducing a power density in target is simultaneously solved. For the obtain of a flux density and neutron spectrum produced by such a source under conditions of finite geometry the calculations has been performed by the Monte-Carlo method with use of the MCNP-4A code [15].

Fig.2 shows the radial distributions of neutron flux in planes remote from the target at distances 3 *cm* and 10 *cm* for the proton energy of 1896 *keV* and a current of 10 *mA*. In the first case, the maximum value of neutron flux is $6.5 \times 10^{9}\ cm^{-2}s^{-1}$ and diameter at 0.1 of maximum ~ 7 *cm*. In the second case, the neutron flux of $10^{9}\ cm^{-2}s^{-1}$ and the characteristic beam diameter of 20 *cm* are achieved.

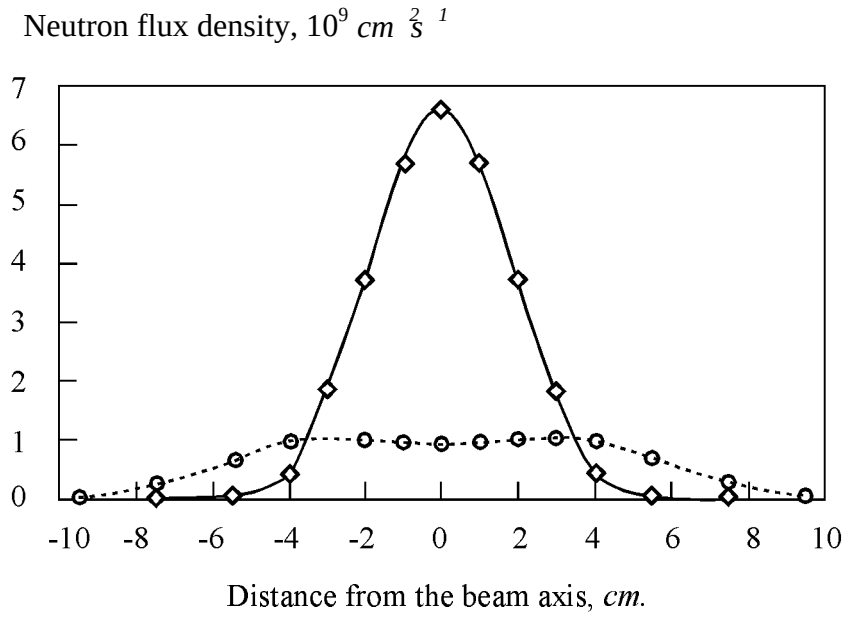

Figure 2. The radial distributions of neutron flux in planes remote from the target at distances 3 cm (◊) and 10 cm (○) for incident proton energy of 1896 keV and beam current of 10 mA.

The calculations of spatial distribution of an absorbed dose performed with MCNP-4A code have shown that such a neutron source at a distance between the object and target of 3 *cm* can produce at a depth $5 \div 7$ *cm* the required therapeutical dose of 20 *Gy* in the exposition of 10 *min* duration. The more detail calculations enable the choice of optimum operation conditions of the source. However, the bench computation has shown the promising for NCT use of the naturally collimated beam of neutrons from the reaction ^{7}Li$(p,n)^7$Be in the near-threshold region under the conditions of open geometry. The accelerator main parameters required for the development of such a source are the following:

- proton energy $E_p = 2$ *MeV*,
- energy stability 0.1 %,
- proton beam current 10 *mA*,
- beam current density 0.5 *mA/cm*.

1.3 ^{7}Li(p,n)^{7}Be Reaction as a source of Epithermal and Fast neutrons

With an increase in proton energy the neutron flight angle is turned by $4\pi\ rad$ at E_p = 1920 keV and the total neutron yield increases up to $1 \times 10^{13}\ s^{-1}$ at an energy of protons 2.5 MeV and a beam current of 10 mA. At such intensity it turns to be possible to produce the source of appropriate to NCT epithermal neutrons by the formation of the required spatial-energy distribution of neutrons with the help of the compact moderator-collimator unit. The design and optimization of such a unit requires the initial data on the spatial-energy distribution of primary neutrons from the thick lithium target. The data can be found out with the use of the following relations:

$$Y = \frac{6.19\left(\frac{d\sigma}{d\omega}\right)}{\left(\frac{dE_p}{dx}\right)\left(\frac{dE_n}{dE_p}\right)},$$

where Y — DDY [$neutron/(eV\ sr\ \mu C)$], $d\sigma/d\omega$ — is a differential cross-section of the reaction ^{7}Li(p,n)^{7}Be [mb/sr],

$$\frac{dE_n}{dE_p} = \frac{(\cos\psi + Z)}{(M_{Be} + M_n)^2}\left[M_p \cdot M_n(\cos\psi + Z) + \frac{M_{Be} \cdot M_{Li} \cdot 1881}{Z \cdot E_p}\right],$$

$$\frac{dE_p}{dx} = \frac{718}{E_p}\left[\ln\frac{E_p}{3000} + 4.96\right],$$

$$E_n = \frac{M_p \cdot M_n}{(M_{Be} + M_n)^2} E_p (\cos\psi + Z)^2.$$

The values of differential cross-section of ^{7}Li(p,n)^{7}Be were quite exactly measured in the broad region of proton energies and then evaluated and summed in tables by Liskien and Paulson [17]. These relations enable the calculation of an absolute yield and the spatially-energy distribution of neutrons from this reaction within the proton energy range over 1920 keV.

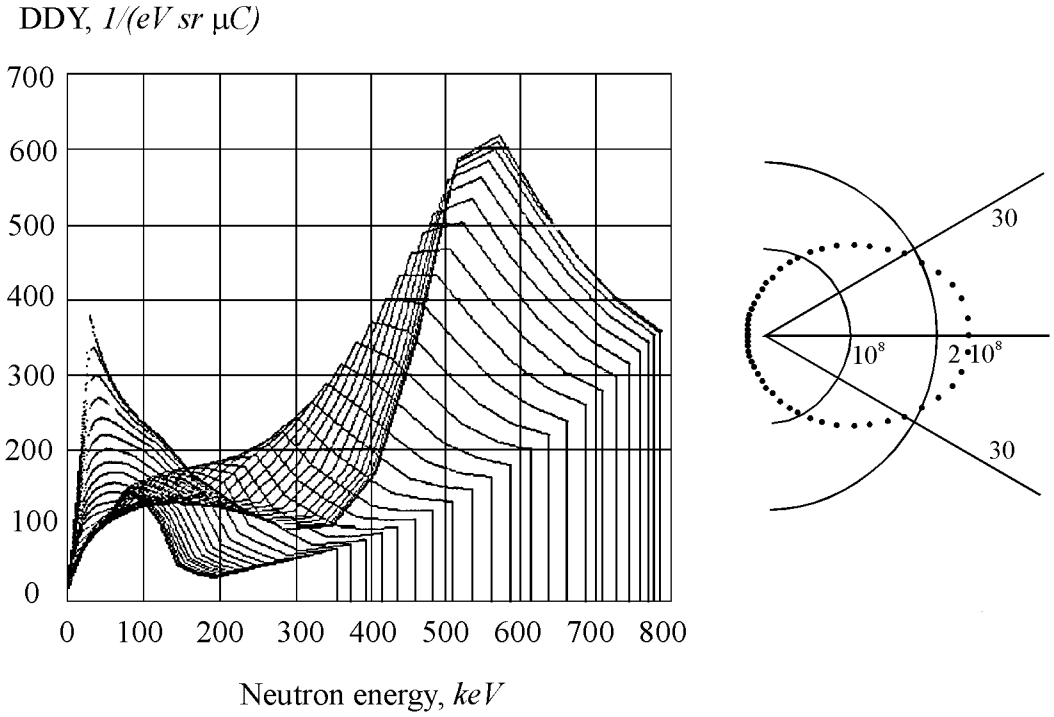

Figure 3. The doubly differential yield of neutrons from thick metallic lithium target for various laboratory escape angle (angle step is 5°) and angular distribution of neutrons in polar coordinates at an initial proton energy of 2.5 MeV.

Fig.3 shows the calculation results for DDY neutrons from the thick lithium target at proton energy of 2.5 *MeV*. The calculations of the spatial-energy distribution of the absorbed dose performed for the optimum moderator-collimator unit with an output window made of the beryllium oxide of 20 *cm* in thickness have shown that such a version of the source of epithermal neutrons for NCT provides the absorbed dose 20 *Gy* at a depth of 5 ÷ 7 *cm* during the exposition of 100 *min*.

The reaction ^{7}Li(p,n)^{7}Be at an energy of protons of 2.5 *MeV* is also the convenient source to FNT. In this case, one has to use the neutrons moving ahead with no attenuation. Such a source can be arranged by putting the target into the compact safeguard unit made of LiH having the collimating-output window.

Fig.4 shows the comparison of neutron spectra normalized to 1 from such a source and B-3 neutron beam of BR-10 reactor widely used for FNT. It is seen that neutron spectra are quite close and the radiobiological efficiency of fast neutrons from ^{7}Li(p,n)^{7}Be reaction should be close to that of the B-3 beam reactor neutrons. The fast neutron flux from the reaction

^{7}Li(p,n)^{7}Be at the proton energy of 2.5 *MeV* and beam current of 1 *mA* at a distance of 20 *cm* from the target is 4×10^{8} *cm* $^{-2}$ *s* $^{-1}$, i.e. it has the same value as that for the B-3 beam.

The requirements to accelerator for producing the source of epithermal neutrons and the source of fast neutrons are the following:

- Proton energy 2.5 *MeV*,
- Energy stability 20 %,
- Beam current of the source of epithermal neutrons ≥10 *mA*,
- Beam current of the source of fast neutrons 1 *mA*.

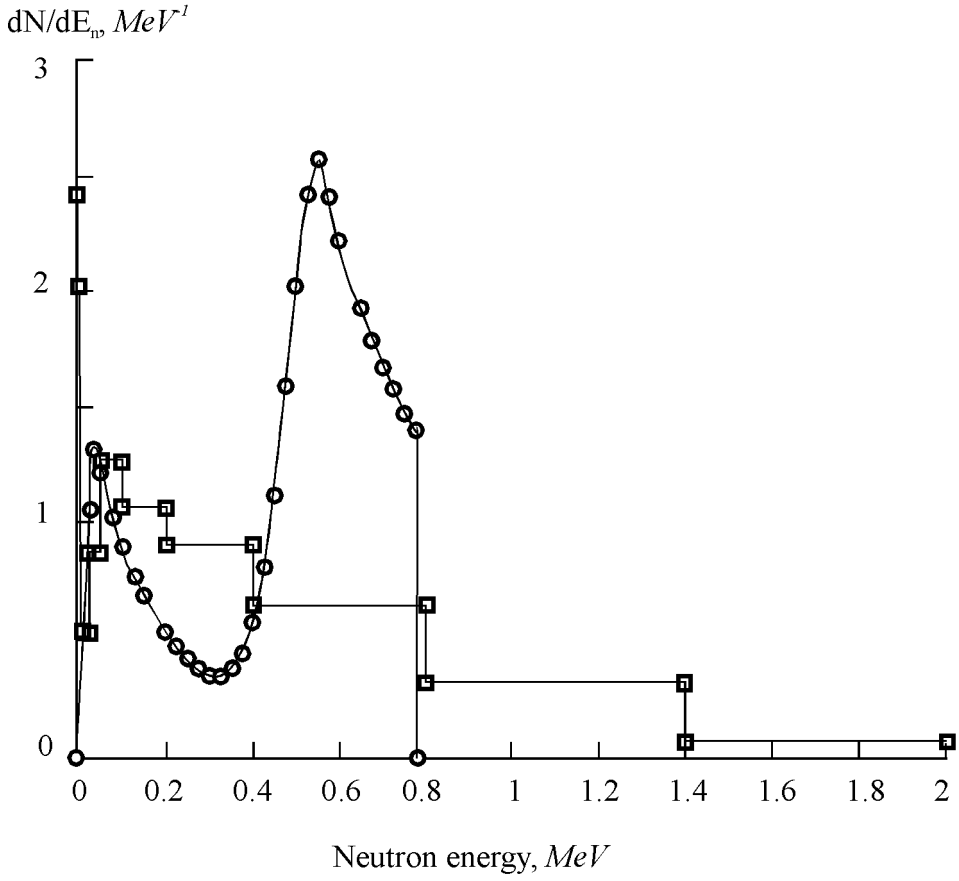

Figure 4. Energy neutrons spectrum for ^{7}Li(p,n)^{7}Be reaction at 0° laboratory angle and initial proton energy 2.5 MeV and neutrons energy distribution for BR 10 reactors medical neutron beam B 3.

1.4 Nuclear-Physics Characteristics of Metal Lithium Target for Obtaining Neutrons

The proton's range with the energy of 2.5 *MeV* in metallic lithium is equal to 300 μm, and up the threshold of ^{7}Li$(p,n)^{7}$Be reaction they are stopped in a 100 μm thick lithium layer. This data should be taken into account in the design of the target. The target can be made either by surfacing or vacuum evaporation onto sublayer. Evaporation can be done directly in the accelerator vacuum cavity thereby avoiding the oxide and nitrite layers on the working surface which appear inevitably at the contact of lithium with air.

The product of nuclear reaction ^{7}Li$(p,n)^{7}$Be is the radioactive nuclide ^{7}Be having half-life time of 53.5 days. A 90 % decay of ^{7}Be proceeds by the radiationless K-capture but in a 10 % by the positron decay accompanied by emitting of gamma-rays with an energy of 0.477 *MeV*. Thus, the irradiated target is a source of gamma radiation with energies 0.477 and 0.511 *MeV*. The activity after an hour exposure by 10 *mA* proton current is 2.33×10^{19} *Bk*, i.e. ~ 60 *mCi*. Such an activity of irradiated target is not a serious radiation danger neither from the point of view of target maintenance nor from the patient's point of view. However, this activity should be taken into account in the work with the target since the contact with air produces the lithium volatile compositions.

In addition to neutron reactions, at the bombardment of ^{7}Li by protons the nuclear reactions occur emitting gamma rays: ^{7}Li$(p,p',\gamma)^{7}$Li and ^{7}Li$(p,\gamma)^{8}$Be the first reaction, gamma-rays of energies 0.477 *MeV* are emitted, in the second reaction, the hard gamma-rays with energies 14.7 *MeV* and 17.6 *MeV*. The output of hard gamma rays is negligible. The output of gamma rays with energy 0.477 *MeV* from thick lithium target with proton beam current 10 *mA* and energy 2 *MeV* is $2.5 \times 10^{11}\ s^{1}$. When irradiating in open geometry for distance to object 3 *cm* the absorbed dose caused by gamma rays from ^{7}Li$(p,p')^{7}$Li reaction with energy 0.477 *MeV* end exposure time 10 *min* will be 4 *Gr* at 10 *mA* proton current, i.e. not more than 5 % of necessary therapeutical dose that considers admissible. With using of source of epithermal neutrons for NCT, produced by moderating of neutrons from ^{7}Li$(p,p')^{7}$Li reaction with protons energy 2.5 *MeV* there is additional possibility of attenuation of gamma rays by means of lead or bismuth shielding around the target. Such shielding with thickness 1.5 *cm* decreases the absorbed dose of gamma rays in 15 times and the space-energy distribution of

neutrons is not affected by this protection. If necessary lead or bismuth shielding can be used in the source of fast neutrons for FNT, also.

It should be noted that target design must exclude a hitting of beam or scattered protons in materials with low nuclear energy levels. For this aim the inner surface of ion-guide should be covered by materials with high (p,p') reaction threshold-graphite, for example.

2. Main elements and arrangement of accelerator complex

Selecting the variant of accelerator for neutron source, it's desirably to provide the possibility of operation in two regimes, considered before, both in the near threshold region allowing to use the source for irradiating in open geometry without external collimator and for generating of epithermal and fast neutrons with protons energy 2.5 *MeV* with moderators. But in spite of attractiveness and elegance of operation in the near threshold region such method of neutron-production demands a high monochromaticity and stability of energy of proton beam (dE/E=0.1 %). This demand makes impossible the use of widely discussed variant of high frequency accelerator of RFQ type and may be satisfied only for electrostatic one.

In this project we offer to create the neutron source based on the construction of vacuum insulation tandem accelerator developed at BINP using the sectionalized rectifier from electron accelerator of ELV type as a powerful source of high voltage. This kind of accelerators (ELV) was developed at BINP and now is in serial production. Advantages of tandem in comparison with accelerator on full energy from the point of providing maximum reliability in works with high current continuous beam are obvious: the ion source is placed under ground potential and the operating voltage is only the half of full proton energy $V \leq 1.25$ *MeV*. The design of vacuum insulation tandem discussed in details in section 3. provides the reliability significantly exceeding the reliability of tandem based on accelerating columns with ceramic insulators, also. The reliability of high voltage ELV rectifier was confirmed by many years of operation of such accelerators in industry. More than 70 of ELV type accelerators were delivered by BINP for operation in Russia's industry and abroad. The use of such rectifier as a high voltage source for tandem supplying is attractive also by its high efficiency (more than 90 %) and for power of proton beam exceeding 20 *kW* it is enough important factor for work in hospital. Design of such transformer and possibility to obtain 0.1 % voltage stability are discussed in details in section 4.

Possible variant of accelerator complex arrangement is performed at Fig.5. The whole installation is placed in two-floor building in four separate rooms. The high voltage source (HVS) and main powerful power supply sources are mounted in one of the rooms (I) of the first floor. The accelerator-tandem is mounted through the hole in ceiling above the HVS, so that its main part — vacuum tank with inputting insulator, potential electrodes and charge-exchange target is situated at the second floor (II). The axis of accelerated and injected beams

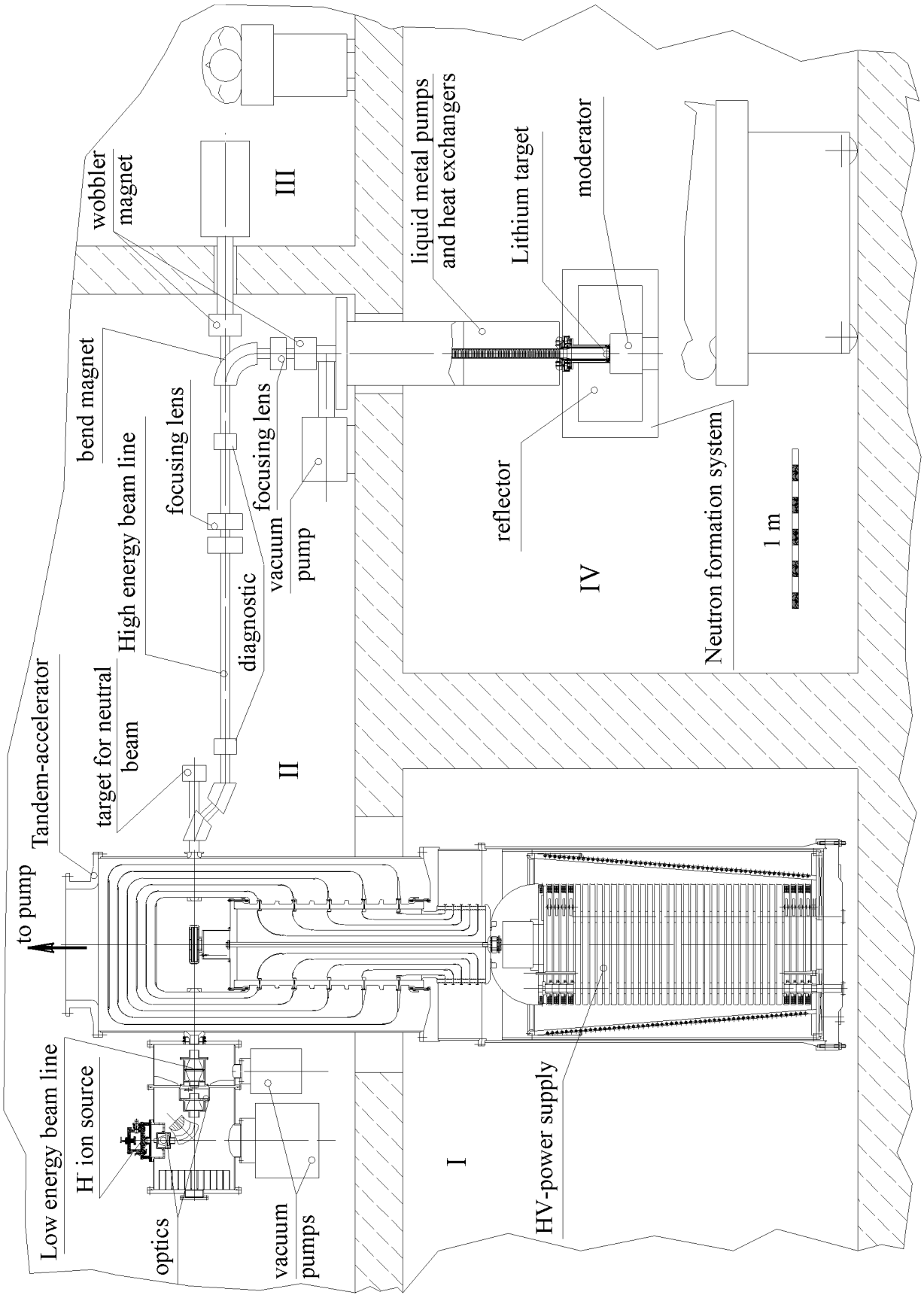

Figure 5. Possible variant of accelerator complex.

have about 1 *m* distance above the floor of the second floor. From the one side of accelerator the source of H^- with differential vacuum pumping system and the optical system of beam transport for injection in accelerator are placed. The beam after charge-exchange process accelerated up to 2.5 *MeV* (doubled energy) comes from the other side of tandem and then the parallel shift system displaces the beam to the transport channel. This system separates the high intensity proton beam and low current beam of neutrals which can be used both to control the efficiency of charge- exchange process and for precise measurements (after additional stripping) of beam energy by means of special bending magnets.

Proton beam is directed by transport channel (high energy beam line at Fig.5) in two medical rooms. The horizontal beam enters the medical room III for works with vertical jet liquid lithium neutron producing target. The heat removal of power released by proton beam is realized by pumping of liquid lithium through the heat exchanger. The transport channel has 90° bending magnet which directs the beam through a hole in the floor to another neutron-producing target situated in the irradiation room IV at the first floor. This target is a tungsten disk cooling intensively by water or liquid metal coolant and covered by thin layer of lithium on which proton beam is thrown. Such target can operate both with solid and liquid lithium, therefore it can be used only with vertically directed proton beam.

Lithium neutron-producing targets are described in details in section 6. They are the most responsible and stressed elements of the whole complex, because all the power of proton beam (more than 20 *kW*) is dissipated in the thin lithium target.

To obtain an uniform distribution of beam on the surface approximately 5 *cm* in diameter a method of recirculating scanning by means of wobbler magnet is used. This magnet is a rotating dipole of cobalt-samarium magnets. Possibility of applying of two variants of target is foreseen — the open target to work in the region near threshold and the target with moderator and reflector. The moderator and reflector are used for space-energy forming of epithermal neutron beam and consist of combination of cylindrical shape blocks filled with D_2O, BeO, MgO, Al_2O_3 (Fig.19). The composition and size of moderator-reflector were optimized by neutron-physical calculations using MCNP program complex. Such work was carried out in several scientific centres (MIT, Ohio Univ, Univ. of Birmingham [10,11,18]). The experimental studying of space distribution of neutrons of this source in fantom had place also. It's planned to continue works under optimization of moderator-reflector to specify its design and composition.

3. High current accelerator-tandem with vacuum insulation

In the conventional scheme of the tandem, two accelerating columns based on ceramic tubes are connected by the high voltage parts with the charge exchange target in between. The prospect of the high current (a few tens milliamperes) accelerator design according to this scheme is limited by its two basic disadvantages — the necessity of pumping the gas charge exchange target through accelerating columns and an inevitable current emission of secondary electrons and ions from the high current beam passage region to the inner surface of ceramic insulators. Both these factors reduce substantially the high voltage strength of accelerating columns and require the substantial increase in their transverse and longitudinal dimensions.

In the tandem developed by us there are no ceramic accelerating columns. In this scheme, to the cylindrical potential electrode with charge- exchange target, placed into vacuum tank, high voltage is applied through ceramic inputting insulator which, in principle, can be arbitrarily remote from the accelerated beam passage region.

The high voltage electrode is surrounded by system of different potential shields providing the homogeneous distribution of the potential and preventing the full voltage effects. In the walls of vacuum tank, potential electrode and in the shields are coaxial round holes for the beam passage which is accelerated and focused during its passage. Since the thin- wall shields placed along the equipotential surfaces of the electrostatic field do not contribute into focusing, the beam focusing in this system is only provided by two axisymmetric lenses - by the lens strongly focusing the low energy beam in the input hole of the grounded wall of vacuum tank and by the lens defocusing the already accelerated beam placed in the hole of potential electrode. The specific feature of such a focusing system with high rate of acceleration is considered below in more details (sect.3.1).

The efficient pumping of the inner cavity of the potential electrode with the gas target placed inside is produced through its upper cover and through removable covers of cylindrical shields. These covers made of vacuum transparent because have a large number of sector holes displaced with respect to each other along the azimuth so to prevent the direct passage and acceleration of particles.

The charge exchange target is a pipe with an inner hole of 4 *mm* in diameter and 260 *mm* in length. In the center of pipe, the gas (nitrogen, air) leaks at a rate providing the efficient density of the target 3×10^{16} *mol/cm*^{2} required for the charge exchange. As shown in sect.3.2, in the geometry under consideration at a given rate of gas leak, the pressure distribution in the whole volume, required for the high voltage strength of a gap, is provided at a pumping rate ~2500 *l/s*.

The most important component of an accelerator is the high voltage inputting insulator through which the potential is transferred into the vacuum cavity from the tank filled with SF_6 gas with the transformer of the ELV-type industrial accelerator being the powerful source of high voltage. The high voltage input is a thick wall ceramic tube of 45 *cm* in diameter and 120 *cm* in length with five metal rings fixed on its outer surface for the fixation of cylindrical shields surrounding the central potential electrode. The potential electrode is placed on the insulator end on the metal flange which is vacuum tightened to the end of ceramic tube by the tightening rod passing along its axis connected to the high voltage source. On the opposite side of the input (placed in SF_6) the rod is tightened to the second end flange supported by the nonvacuum part of insulator formed of 6 rings of organic glass separated by metallic rings for the potential distribution. The voltage is applied to these rings from the resistive-capacitive divider providing the homogeneous distribution of the potential along the insulator length. Inside the insulator around the tightening rod five thin wall pipes of various lengths are concentrically located to connect the respective rings of different potential on the vacuum ceramic part of the insulator and its lower part placed in SF_6 gas.

The radial gaps between the cylindrical shields in the vacuum part of accelerator are selected to be of 4 *cm* so that at the voltage of 1.25 *MV* on the potential electrode the potential difference between shields is ~200 *kV* and the maximum electric field intensity does not exceed E_{max}= 60 *kV/cm*. The field intensity on the surface of ceramic insulator, divided along its length by 6 metal rings into 6 sections by 20 *cm* each, is less than 10 *kV/cm*. In the insulator inner part filled with SF_6 gas, the radial separation of the potential around the central tightening rod is provided by the thin wall cylindrical tubes and their geometry is selected in such a way that the maximum field intensity in SF_6 gas at pressure of 3 *atm* does not exceed 70 *kV/cm*. Such intensities of electric fields seem to be quite moderate so one can expect very reliable operation of the high voltage input from the viewpoint of the electric strength. As an insulator it is

Figure 6. Photo of the tandem prototype.

planned to use a widely used in electrotechnical industry ceramic insulator of the type P1240/450 UHL1 which needs a slight modification for fitting and connection of the inner and outer metal rings fixing the cylindrical shields of potential separation.

The prototype of such a tandem with vacuum insulation at an energy of 1 MeV is presently used successfully as an injector of the compact proton synchrotron (Fig.6 view of synchrotron).

The high voltage source is a cascade multiplier at voltage of 0.5 MeV. The potential electrode is surrounded by two shields with the 3 cm gaps and voltage of 170 kV between each other. The tandem is operated with a pulse source of negative ions providing the current up to 8 mA at a pulse duration of 10 μs. At present, as the charge exchange target a pulse gas (air) target is used. This is a 16 cm long pipe with the inner diameter of 0.8 cm with a pulse (1 ms) gas pumping in the center of the tube. The stationary gas target being tested on the special vacuum stand is planned to be installed on this tandem.

3.1 Tandem optics

The specific feature of the tandem optics is determined by the design of its potential electrodes. The edges of round holes in the walls of the input grounded, and potential electrodes have roundings to eliminate the higher intensities of electric field. At the same time, the electrodes with the distributed potential, the repeating equipotential field surfaces are desirably to be made of minimum thickness for eliminating the transverse components of the field in the holes generating the excessive intensities and beam focusing. From the design viewpoint their thickness was chosen to be 1 *mm*. This enables the minimum gap between the potential electrode and the grounded tank wall determined only by the admissible field intensity between the electrode metal surfaces and also enables one to provides the maximum rate of particle acceleration. In the geometry selected the total energy growth $E = 1.25\ MeV$ is achieved at a length of 24 *cm*. The energy of H^- ions injected into the tandem is 25 *keV*.

The second specific feature of the tandem is that there is only one strongly focusing lens of the tandem input hole where the particle energy is still low. The second (defocusing) lens in the potential electrode input hole is weak since here the beam has already high energy. The high rate of acceleration reduces the longitudinal size to its minimum in the area of the input lens where the space charge has a substantial effect. The focal distance of the input lens is determined by its hole diameter. Fig.7 shows dependencies of the focal distance (a distance to the axis intersection point from the tank inner surface) on holes diameter.

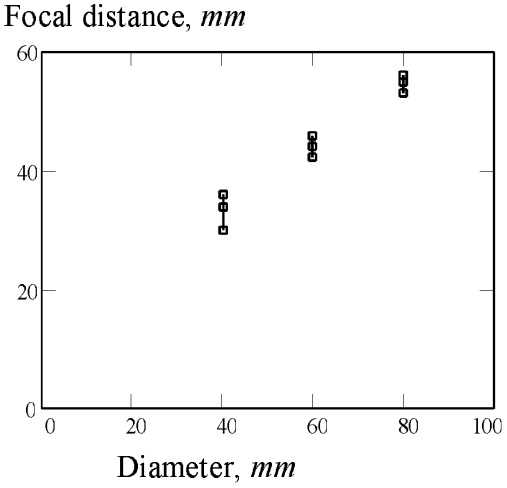

Figure 7. Dependencies of the focal distance(a distance to the axis intersection point from the tank inner surface) on holes diameter. The particles direct backward from the second shield in parallel to the axis (point from above - radius 5, 10 and 15 mm).

The lens focal distance increases if the hole in the thick wall is made not of round but the cone shape. In our geometry, diameter of all the holes are selected to be of 50 *mm*, the input hole on the output shifts to the cone with resultant of 45° and a base of 110 *mm*. As a result, the lens focus is placed at a distance of 80 *mm* from the tank inner surface (the tank inner diameter is 530 *mm*). The crossover for the converging beam transported from the outer source of negative ions should be located here. For each current value the optimal convergence angles should be conform with the beam divergence from the crossover under the action of space charge. Fig. 8a shows the characteristic particle trajectories in the tandem. The upper curve is the laminar flow boundary of 50 *mA*. Fig.8b shows the boundary of the nonlinear beam and the longitudinal electric field diagram.

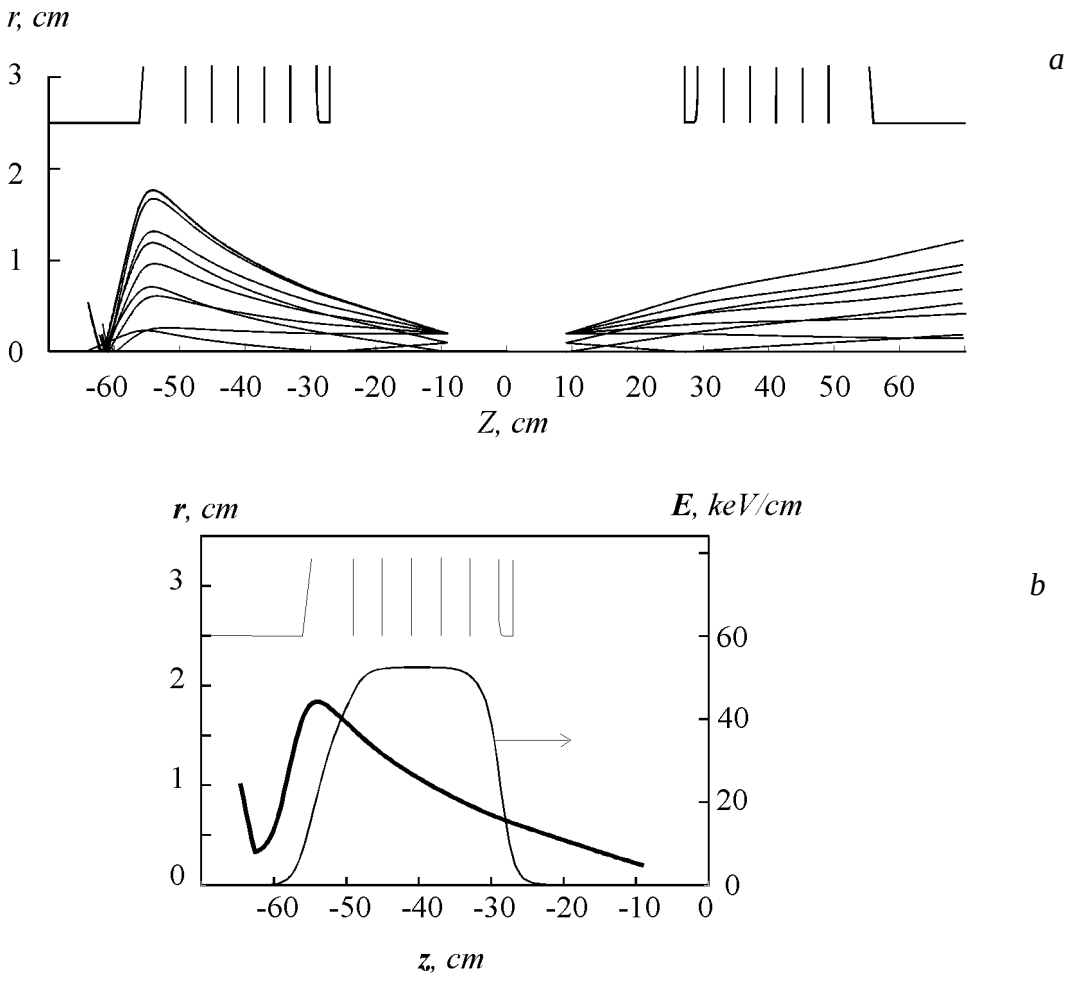

Figure 8.

a — The characteristic particle trajectories in the tandem without regard for space charge and the boundary of 50 mA laminar flow (the upper curve is in the range of negative z);

b — The boundary of nonlinear 50 mA beam. A diagram of longitudinal electric field is also shown. Note that longitudinal and transverse scales differ. The electrode surfaces are shown in the area r ≥ 2.5 cm.

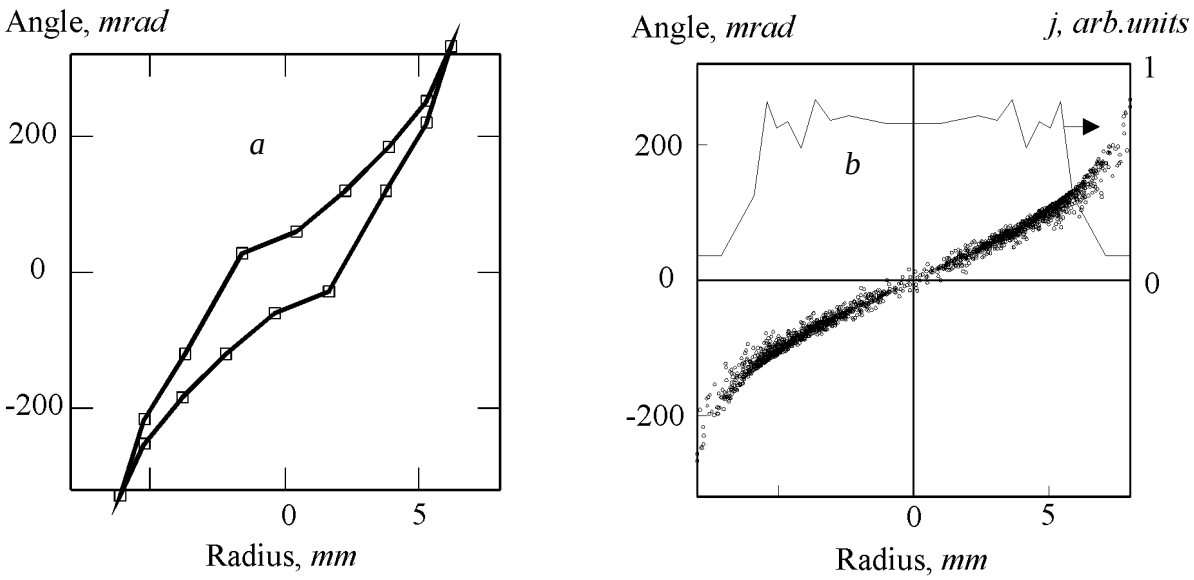

Figure 9.
a — Charge exchange tube acceptance *without regard for space charge in front of input lens (on distance of 60 mm from the tank inner surface);*
b — 50 mA beam emittance with homogeneous distribution of current density in charge exchange tube in front of input lens (on distance of 60 mm from the tank inner surface).

Tandem acceptance

The tandem acceptance is determined by the geometry of the charge exchange target which has the form of the tube of 180 *mm* in length and 4 *mm* in diameter. The tandem acceptance in front of the input lens without regard for space charge of a beam is given in Fig.9a (it is obtained by the backward passing of target acceptance through the input and output lenses). The acceptance shape distortion is the result of spherical aberration of lenses. The emittance diagram of 50 *mA* beam in front of the input lens is given in Fig.9b. The beam will have homogeneous distribution of current density in charge exchange target.

Comparison of tandem acceptance without regard for space charge (Fig.9a) and the one with consideration for space charge of 50 *mA* beam (Fig.9b) shows the tandem optics to have low sensitivity to current.

Effect of shields with distributing potential

At the finite thickness of a shield, its hole is operated as a weak focusing lens. The focusing effect of shields is numerically calculated for the thickness of 1 *mm*, the hole diameter of 50 *mm* and the gap between shields of 40 *mm*. For finding out the effect of an individual shield it was assumed that the previous and next shields have no holes. Particles from the previous shield directed in parallel to the axis with different transverse coordinates upon passage the hole acquire the small diverging angle which is practical linearly dependent of the coordinate, i.e. the hole in the first shield acts as a lens with large focal distance of 30 *m*. All the next lenses has lower affect on the beam because of the energy increase.

Effect of shield curvature

The shields have the shape of cylinders that leads to the appearance in one plane of radial electric field focusing the beam. For the first shield, the focal distance of the generating lens is turned to be 4 *m* that influences weakly on the beam focusing during the passage of tandem. This focal distance can be increased by local decreasing of shield curvity.

3.2. Charge exchange target

The effective pumping of the inner cavity of the potential electrode with the gas target located inside is performed through its upper cap and through the caps of cylindrical shields. The holes in caps are blocked by the symmetrically located sectors. The sectors of the neighboring caps are shifted along the azimuth so to prevent the direct passage of accelerated particles since this might cause the multiplication of accelerated particles due to the secondary emission.

Description of charge exchange target

The charge exchange target is a tube with its inner diameter of 4 *mm* and 260 *mm* in length. In the center of the tube, the gas filling is performed providing the target density required for the charge exchange. The process of charge exchange of negative ions is related to the process of the charge exchange of protons into neutral particles, protons into negative ions, neutral particles into protons, neutral particles into negative ions, negative ions into neutral particles, and negative ions into protons with cross-sections σ_{10}, $\sigma_{1\text{-}1}$, σ_{01}, $\sigma_{0\,1}$ $\sigma_{1\,0}$, $\sigma_{\text{-}11}$, respectively. At a particle energy of 1 *MeV* the following in equalities take place $\sigma_{1\text{-}1} << \sigma_{10} << \sigma_{0\,1} << \sigma_{\text{-}11} < \sigma_{01} < \sigma_{\text{-}10}$. Neglecting the processes of the electron capture we get the dependence on the proton concentration on the target thickness δ.

$$\theta_+ = 1 - \frac{\sigma_{-10} - (\sigma_{01} - \sigma_{-11}) \cdot e^{-(\sigma_{-10} + \sigma_{-11} - \sigma_{01})\delta}}{\sigma_{-10} + \sigma_{-11} - \sigma_{01}} \cdot e^{-\sigma_{01}\delta}.$$

Using the experimental data on the charge exchange cross-sections: $\sigma_{11}=0.47\cdot10^{-16} cm^2$, $\sigma_{01}= 1.54\cdot10^{-16}\ cm^2$, $\sigma_{10}= 3\cdot10^{-16}\ cm^2$ for nitrogen, $\sigma_{11}=0.84\cdot10^{-16}\ cm^2$, $\sigma_{01}= 1.26\cdot10^{-16}\ cm^2$, $\sigma_{10}= 1.6\cdot10^{-16}\ cm^2$ for magnesium, and reasoning from the necessity to provide 99 % yield of protons one can find the target thickness for nitrogen $\delta_N=3.3\cdot10^{16} cm^{-2}$, for magnesium $\delta_{Mg}=3.9\cdot10^{16}\ cm^{-2}$.

We can find the ionization losses of energy $\Delta\omega$ using the Bete formula [19]:

$$\Delta\omega = \varepsilon\delta, \qquad \varepsilon = 8\pi a_0^2 Z \cdot I_i \cdot \left(\frac{\alpha}{\beta}\right)^2 \left[\ln\left(\frac{4I_i}{ZB}\cdot\gamma^2\cdot\left(\frac{\beta}{\alpha}\right)^2\right) - \beta^2\right],$$

$\Delta\omega = 177.8\ eV$ for nitrogen, $\Delta\omega = 306.6\ eV$ for magnesium.

The mean square of energy loss dispersion on the path of 1 $atom/cm^2$ is:

$$\Delta W = 16\pi a_0^2 Z \cdot I_i^2 \cdot \left[1 + \frac{ZB}{2I_i}\left(\frac{\alpha}{\beta}\right)^2 \cdot \ln\left(\frac{4I_i}{ZB}\cdot\left(\frac{\beta}{\alpha}\right)^2\right)\right].$$

The mean dispersion of energy losses on the whole path is: $W = \sqrt{\Delta W \delta}$. W = 275 *eV* for nitrogen, W = 406 *eV* for magnesium.

Calculation of gas consumption

The tube conductivity is calculated for the molecular regime by the formula $U = \frac{\pi}{12}\cdot v_a \cdot \frac{d^3}{L}$, where d and L are diameter and length of tube, $v_a = \sqrt{\frac{8kT}{\pi m}}$ is velocity. $U(x)$ = 1.23 ·10^4 d^3/L for nitrogen at T = 293°*K*. $U(x)$ = 1.33 ·10^4 d^3/L for nitrogen at T = 693°*K* (d and L in *centimeters*, U in cm^3/c).

The gas flow from the center to the tube edge is Q = [*P(x)* *P(0)*]·*U(x)*, where $U(x) = \frac{\pi}{12}\cdot v_a \cdot \frac{d^3}{x} = \frac{U_0}{x}$, $U_0 = 1.23\cdot 10^4 \cdot d^3$ for nitrogen, $U_0 = 1.96\cdot 10^4 \cdot d^3$ for magnesium. Neglecting the pressure on the tube edge *P(0)*, one can write the pressure distribution over the tube as following:

$$P(x) = \frac{Q}{U(x)} = \frac{Q\cdot x}{U_0}.$$

The target thickness is:

$$\delta = 2C\int_0^l P(x)\cdot dx = 2C\int_0^l \frac{Q\cdot x dx}{U_0} = 2\cdot\frac{C\cdot Q}{U_0}\cdot\frac{l^2}{2},$$

where $l = L/2$ is a half of the tube length, C is the number of gas molecules in 1 cm^3Torr. $C = C_{N_2} = 3.4\cdot 10^{16}\ cm^{-3}Torr^{-1}$ for nitrogen at 20°*C*, $C = C_{Mg} = 2.2\cdot 10^{16}\ cm^{-3}Torr^{-1}$ for magnesium at 400°C.

So, the gas consumption necessary for the given target thickness is:

$Q_{N_2} = \frac{\delta_{N_2}\cdot 1.23\cdot 10^4 d^3}{C_{N_2}\cdot l^2}$ for nitrogen, $Q_{Mg} = \frac{\delta_{Mg}\cdot 1.96\cdot 10^4 d^3}{C_{Mg}\cdot l^2}$ for magnesium.

Table 3 shows the values for Q and also for the pressure in the center *P(l)* and on the output *P(0)* of the tube at δ_{N_2} =3.3·10^{16} cm^{-2} and δ_{Mg}=3.9·10^{16} cm^{-2}.

Table 3.

	N_2		Mg	
L, cm	26	18	26	18
Q, cm³Torr/s	4.5	9.4	13.4	28.4
P(l), Torr	3.8×10^{-2}	5.7×10^{-2}	6.8×10^{-2}	9.8×10^{-2}
P(0), Torr	1.5×10^{-3}	3.1×10^{-3}	4.5×10^{-3}	9.4×10^{-3}

The free path length at $P(l) = 3.8\cdot10^{-2}$ *Torr* for nitrogen is 1.7 *mm* at the effective size of 4 *mm*. The conductivity calculated for the molecular-viscous regime by the formula $U_{mv} = 0.9U + U_v$ [20] (where $U_v = 1.36\cdot10^5 \frac{d^4}{l}\cdot\frac{P(l)+P(0)}{2}$ is conductivity for the viscous regime) differ slightly from *U*.

In a vacuum system, gas emission may also exist due to desorption of gas from surface polluted with adsorbed gases, vapours, remaining water and oil films. Excluding the starting period of operation, the gas emission for polished stainless steel and ceramics is $q_{ss}=3\cdot10^{-9}$ *l·Torr/cm²s* and $q_c=1,1\cdot10^{-9}$ *l·Torr/cm²s*, respectively [21]. With the whole square of the stainless steel surface $A_{ss}= 2.8\cdot10^5$ *cm²* and ceramics $A_c=9.4\cdot10^3$ *cm²*, summary gas emission of walls is $Q_g = 1.1$ *cm³·Torr/s*. The value is expected to decrease in operation hundred times.

Calculation of vacuum system by method of statistic tests

For the calculation of conductivity for components and pressure distribution in the vacuum system the method of statistic tests was employed (the Monte Carlo method). With the statistic simulation of the gas flow in vacuum system a large number of molecule trajectories are traced from the start to the moment of their return to the surface of the input or output or at the moment of saturation if there are the saturating surfaces.

In the program used the only molecular (collisionless) motion of particles is considered. This motion is characterized first of all by the linear trajectory, and second by the specificities in particle interactions with the vacuum chamber walls.

According to that mentioned above the mathematics simulation compresses two independent problems: the first one is the description of particle motion inside the vacuum cavity, and the second is the simulation of particle collision with the wall surface.

The first problem is solved in the following way: the particle motion is considered to be its simple motion from one point of the vacuum cavity surface to another along the direct line.

The particle collision with the surface of vacuum apparatus is characterized by a) its probability to be absorbed, b) probability of the isotopic (within $0 \div 2\pi$) reflection of particles. The simulation particle collision with the wall is performed with the Monte Carlo technique. Introducing the surface properties is determined by giving the dependencies of particle sorbtion probability, probability of the isotropic reflection of particles.

The probability for a molecule to flight out of the surface at the start or at the reflection according to the experimentally established the cosine low is equal to: $dP = A\frac{d\omega}{2\pi}\cos\gamma$, where γ is an angle to the normal, $d\omega = 2\pi \sin\gamma d\gamma$ is an elementary solid angle, $A = 2$ from the conditions of normalization. By the integration from 0 to 2π we get the fraction of molecules flying out inside the angle γ: $\xi = \int_0^{\gamma} dP = \int_0^{\gamma} \sin 2\gamma d\gamma = \sin^2\gamma$. Hence the expression which is used for finding out the random angle $\gamma = \arcsin\sqrt{\xi_1}$, at the generation by the random number transmitter uniformly distributed within the interval from 0 to 1, of the random number x_1. The random azimuthal angle j is uniformly distributed within the interval from 0 to 2π: $\varphi = 2\pi\,\xi_2$.

The capability of the vacuum system component is defined by the probability of the shift of molecules from the input cross-section to the output one. For example, for the calculation of the charge exchange tube capability it is assumed that both the input and output holes are the surfaces with the absorption coefficient to be $K_s = 1$. The injection surface is near the input surface and N particles are injected from the surface (the conductivity coefficient) is defined as $P = N_{out}/N$ where found as a result of calculations. In this case, the tube capacity is equal to:

$$U = U_0 S \cdot P = U_0 S \cdot \frac{N_{вых}}{N},$$

where U_0 is a capacity of 1 cm^2 hole (1.177×10^4 cm/s for nitrogen, 1.956×10 cm/s for magnesium at 400°C), S is the input hole area.

Fig.10 shows various designs of the charge exchange tubes with a 4 mm diameter of the input hole. Arrows indicate the place of particles injection.

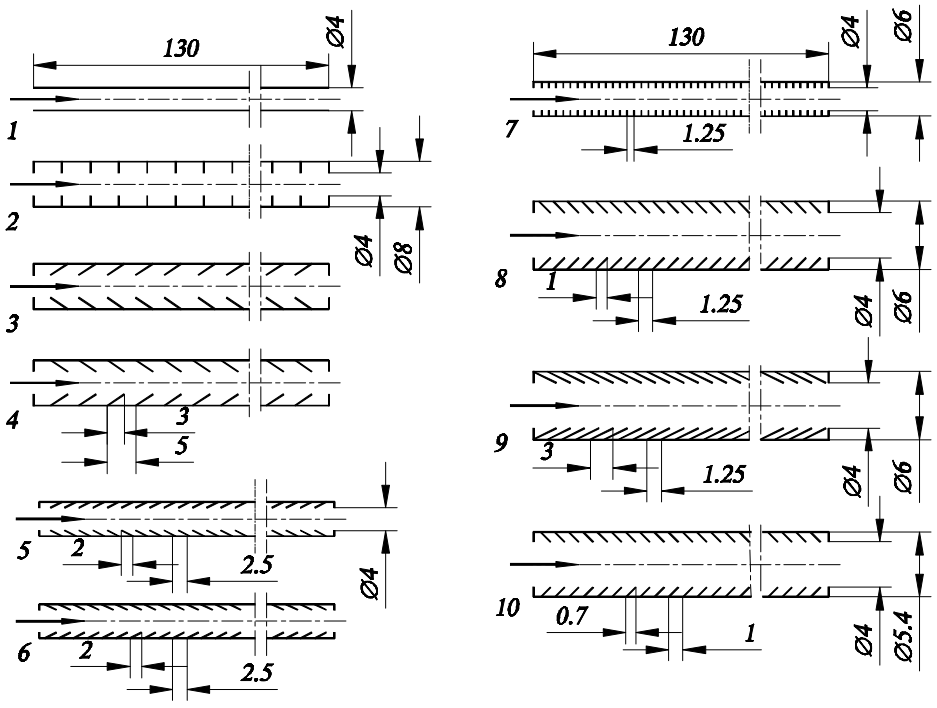

Figure 10. Designs of the change-exchange tubes, have ring partitions (1 ÷ 7 — in scale 1:1, 8 ÷ 10 — in scale 2:1).

The calculation results of the conductivities of these versions for nitrogen are given in Table 4.

Table 4.

№. designs	1*	1	2	3	4	5	6	7	8	9	10
U, cm³/s	60.6	52.5	61.2	68.0	59.4	60.2	46.3	38.5	35.1	43.1	30.6

** For the comparison, in the first column of Table there is the conductivity value for the first version calculated by the analytical formulae.*

The calculation showed also the tube conductivity to be inversely proportional to their length, so by analogy with analytical calculation the usage of the tube with lowest conductivity will result in decrease of gas consumption by a factor of (52.5/30.6) ≈ 1.7.

For finding out the pressure distribution in the vacuum system it is used the number of collisions (obtained in calculations) of molecules with the surface N_i referred to the surface

area A_i: $P_i = K N_i/A_i$ where K is the coefficient. For the calculation vacuum system the pump input pressure is $P_i = Q/S_i$, where $Q = 4.5\ cm^3\ Torr\ s^{-1}$ - the gas emission in the system, $S_H = 2\ m^3/s$ is the pump rate. $P_H = 2.25\times10^{6}\ Torr$. If the number of collisions with the surface A_H is equal to N_H, $K = P_iA_i/N_i$. With a single pump in the system all injected particles N are absorbed by the surface A_n, and the number of collisions is $N_n = N/f$, where f is vacuum factor of the pump, and $K = f{\cdot}P_iA_i/N$.

The pressure distribution in the vacuum system at the given values is show in Fig.11. The gas flow from the gas charge exchange tube enters mostly to the upper large holes. A and B partitions with the holes of 5 *mm* and 6 *mm* protect the acceleration tract from gas. Calculation shows that in the tract area the pressure exceeds the one shown in the draft less than 10^{7} *Torr*.

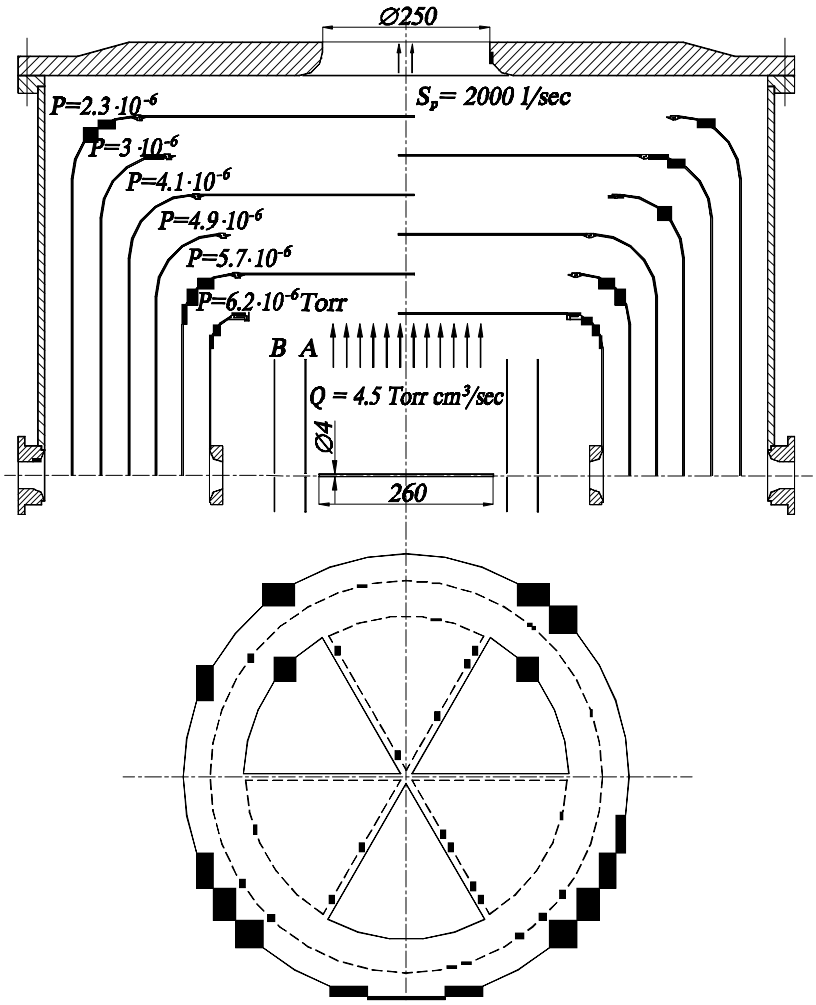

Figure 11. Distribution of pressure in the vacuum system at $Q = 4.5\ cm^3\ Torr\ s^{-1}$.

4. Power high voltage source of accelerator for generation of neutrons for NCT and FNT

In this project is offered to use as the high voltage source the high voltage rectifier of ELV-type accelerators which are used for industrial application.

Before looking the high voltage source we will be concerned with the main parameters of ELV-type accelerators and their constructing features which can be used when the accelerator for neutron generation will be made.

Main parameters of ELV-accelerators

Beginning from 1971, the Budker Institute of Nuclear Physics Siberian Branch of Russian Academy of Science (SB RAS) started its activity in the development and manufacturing of electron accelerators of the ELV-type for their use in the industrial and research radiation-technological installations [22]. The ELV-type accelerators are designed with use of the unified systems and units enabling thus to adapt them to the specific requirements of the customer by the main parameters such as the energy range, beam power, length of extraction window, etc. The design and schematic solutions provide the long term and round-the -clock operation of accelerators under the conditions of industrial production processes. The specific features of the ELV-accelerators are the simplicity of design, convenience and ease in control and reliability in operation.

INP proposes a series of electron accelerators of the ELV-type covering the energy range from 0.2 to 2.5 MeV with a beam of accelerated electrons of up to 200 mA and maximum power of up to 160 kW. By now, over 70 accelerators had been delivered inside our country and abroad and the total operation time exceeds 500 accelerator-years.

Basic parameters of the ELV-type accelerators are given below (Table 5):

Apparently from the table the high voltage rectifiers of our accelerators by its parameters (energy and power) can be used for BNT and BNCT purposes.

Table 5.

	Energy range, *MeV*	Beam power, *kW*	Max. Beam current, *mA*
ELV mini	0.2 ÷ 0.4	20	50
ELV 0.5	0.4 ÷ 0.7	25	40
ELV 1	0.4 ÷ 0.8	25	40
ELV 2	0.8 ÷ 1.5	20	25
ELV 3	0.5 ÷ 0.7	50	100
ELV 4	1.0 ÷ 1.5	50	100
ELV 6	0.8 ÷ 1.2	100	100
ELV 8	1.0 ÷ 2.5	90	50
ELV 6M	0.75 ÷ 0.95	160	200
Torch	0.5 ÷ 0.8	500	800
ELV 12	0.6 ÷ 1.0	400	400

Design

General view of the ELV-type accelerator with a foil extraction is given in Fig.12 and Fig.13. Inside the tank filled with the SF_6 gas are located: primary winding, high voltage rectifier with a built-in accelerating tube, high voltage electrode and the injector control unit. Just the location of the accelerating tube inside the column of high voltage rectifier makes the ELV-accelerators the most compact among the devices of this class. The vacuum system components and extraction device are fixed to the bottom of the tank. Electrons emitted by the cathode, placed on the upper part of the accelerating tube, have the total energy eU_0 on the output of the accelerating tube. Passing through the vacuum system they reach the extraction device where they are homogeneously distributed by the scanning electromagnets and then extracted into air. The irradiated material is transported under the frame of the extraction window.

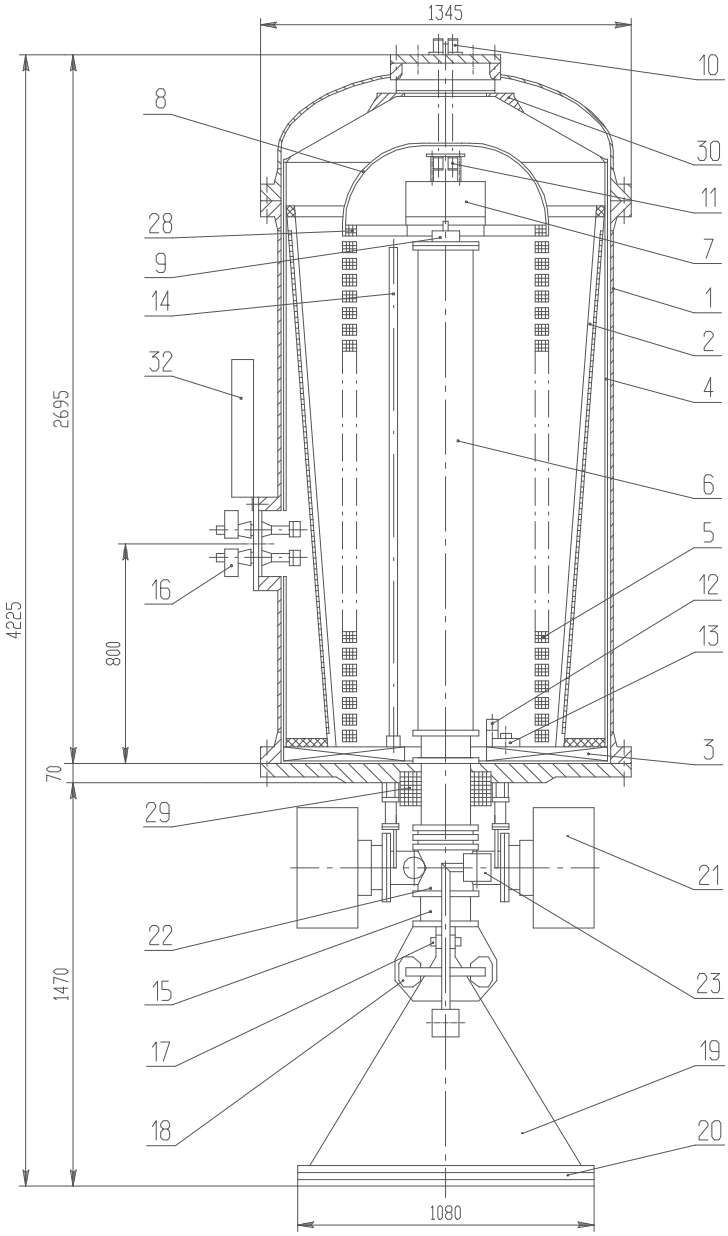

Figure 12. General view of ELV-4 accelerator: 1 - vessel, 2 - primary winding; 3,4 - magnitoguides; 5 - rectifier sections; 6 - accelerating tube; 7 - injector control unit; 8 - high voltage electrode; 9 - injector; 10,11 - optical channels for injector control; 12 - section divider; 13 - capacitor unit; 14 - energy divider; 15 - vacuum gate; 16 - primary winding terminals; 17,18 - scanning coils; 19 - extraction device; 20 - extraction window frame; 21 - vacuum pumps; 22 - cross head; 23 - vacuum gate; 28 - base of high voltage electrode; 29 - magnetic lens; 30 - high voltage shield; 32 - clamp set.

Figure 13. Photo of the accelerator ELV 8.

High voltage rectifier

The source of high voltage is a cascade generator with a parallel inductive coupling. The rectifier section column is installed inside the primary winding. The electric circuit of the section is given in Fig.14. The coil of secondary winding has 3000 turns and maximum voltage induced on its ends is 20 *kV*. This voltage is rectified by the voltage doubling scheme. Thus, the output voltage of the rectifying section is 40 *kV*. The rectifying sections are connected either in series (Fig.14a) or in series-parallel (Fig.14b). The rectifiers with the series connection of sections are of higher voltage and those with the series-parallel connection are of higher current. The rectifier section column is terminated with the high voltage electrode inside of which there is the injector control unit and a special coil for its power supply.

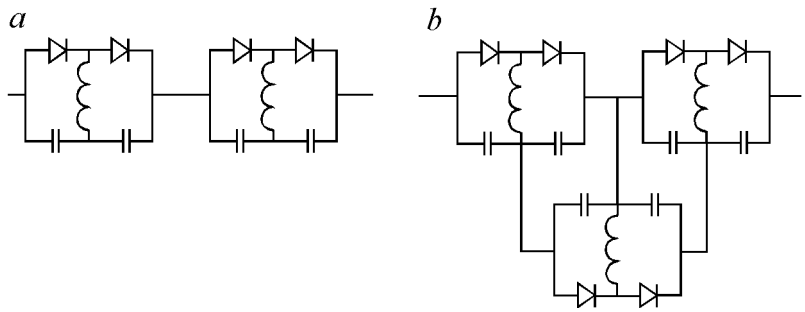

Figure 14. ELV rectifying section circuit and means of their connection.

Note, that compared to the "conventional" transformers in our design there is no central magnetic guide. This circumstance simplifies substantially the high voltage source design does not practically influence on the operational characteristics of the rectifier because of successful design of the primary winding and by the presence of the high quality of the energy stabilizing system and also due to quite low turn voltage (6 *V/turn*). The transformer specific power in the ELV-type accelerators is about 40 *kW/m*.

The use of the low inductive capacitors K-15-10, original scheme of intrasection connections, and the presence of damping resistances provides the reliable protection of components of high voltage rectifier against of overvoltages during break-downs both of vacuum and gas insulation. Generally specking, the break-down in the ELV-type accelerator is

exceptionally rare event, however during the design of accelerator (and this principle is always followed) we assumed that even a great number of break-downs (hundreds and thousands) should not lead to the damage of the high voltage rectifier.

The practice proved the high reliability of the high voltage rectifier.

High voltage source for NCT and FNT

The high voltage sources of the ELV-4 accelerator (tandem version) and ELV-8 accelerator (direct accelerating of protons version) with changing polarity of output voltage are the most convenient .

For tandem version the ELV-4 accelerator rectifier can provide proton beam current up to 20 *mA*. It corresponds to full power 40 *kW*. If you want to increase the proton beam current up to 50 *mA*, (i.e. full current rectifier 100 *mA*), it must be constructed by means of Fig.14b. This construction change is unprinciple and unimportant correction.

The using high voltage sources of ELV-8, will be useful in a case of direct (without recharging) accelerating protons. In this case the max. proton's current is equal to 50 *mA*.

Stabilization of accelerating voltage

The energy stabilization system used in accelerators of ELV-type provides $1 \div 2$ % instability of accelerating voltage. The value of voltage pulse is about 10 *kV*. This stabilization system is enough, if the high voltage source is used for generation BNT neutrons. However, the instability of accelerating voltage should be no more than 0.1 % if it will be used for BNCT. For it:

- it is necessary to design the slowly feedback of stabilization based on measurement of accelerating proton energy;

- it is necessary to design the system active suppression pulses of high voltage source with strip range to be equal a few *kHz*.

Power supply

The power supply of the primary winding of the accelerator is provided by the frequency of 400 *Hz* from the frequency converter. By now, the rotary frequency converters were used which were attractive by the low price, simplicity, and reliability. The only deficiency of these machines is quite low efficiency ($65 \div 80$ % depending on power). The attempts are made now to replace them by the static frequency converters (both the thyristor and transistor types). In this case, the total efficiency is expected to increase up to 85 % for the machines of up to 100 *kW* and up to 92 % for more powerful accelerators.

The thyristor key is designed for the fast ($< 10^{-3}$ *s*) de-energizing the accelerator in case of emergency as: the vacuum or gas insulation break-down, decrease in currents of scanning and lens, foil cooling stop.

All the operative reswitching in the power supply is made by the control program automatically without actions of operator.

The power system is not need in the changes when it work in a complex.

Control system

The control system for the industrial accelerator determines its operation such as its characteristics reliability, continuous operation, repair fitness, level of personnel qualification.

The operator of technological installation is communicated with the accelerator through the computer. The accelerator control system comprises a set of the software and hardware covering all the accelerator units required an operative control and diagnostics. The multifunctional control system enables one:

- to make the automated control of the accelerator. Algorithms introduced into the accelerator control program, solve the problems of the preparation of the accelerator to its operation (speed-up of frequency converter, switch on of the foil blow motor, switch scannings and if necessary, technological equipment), watch the status of blockings and after switching on of the accelerator and install an energy and current of an electron beam in the given regime;

• to stabilize safely the main parameters of an electron beam (electron energy, beam current, size and position of the raster on the foil of the extraction window) which provides the high quality of radiation treatment;

• to provide the continuous diagnostics of the high voltage rectifier and selftesting of the other accelerator systems during the operation of accelerator;

• to synchronize the accelerator operation and technological equipment; in this case, the operation of accelerator integrated into technological line in completely automated regime is possible;

• provides for the personnel a wide choice of commands for the regimes of testing and adjusting the accelerator to be preliminary issued.

Fig.15 shows the functional diagram of the ELV accelerator connections with the control system.

The high voltage rectifier column which consists of the connected in series rectifying sections S_1 ... S_n through the primary winding L_1 takes the power from the frequency converter FC. The high voltage is measured with the help of the energy resistive divider and signal E_0 is applied to the input of the energy stabilizing system ESS. The control action proportional to the difference between the requested and real energy is applied to the excitation winding EW of the frequency converter FC. A long time instability of an energy is in the range of $1 \div 2$ %.

The stabilization of energy and control of power supply PSCS systems make the lower level of the control system — the level of the end control units. All the control commands for giving of modes, etc. are formed on the next level of the control system: the module informatio-measuring system MIMS.

The CAMAC section comprising the required set of measuring and control modules either specialized for the ELV accelerators control station made on the base of microprocessor is used as the module information-measuring system. The station comprises the 64-channel input and output registers, 12-bit ADC with 64-channel analogue multiplexer on the input, 16 12-bit DAC.

On the 3rd upper level of the control system there is the control computer loaded with packet of specialized software. The software of the accelerator control system provides a friendly interface with the user through the system of dynamic menus, text and graphic visualization of the accelerator operation run.

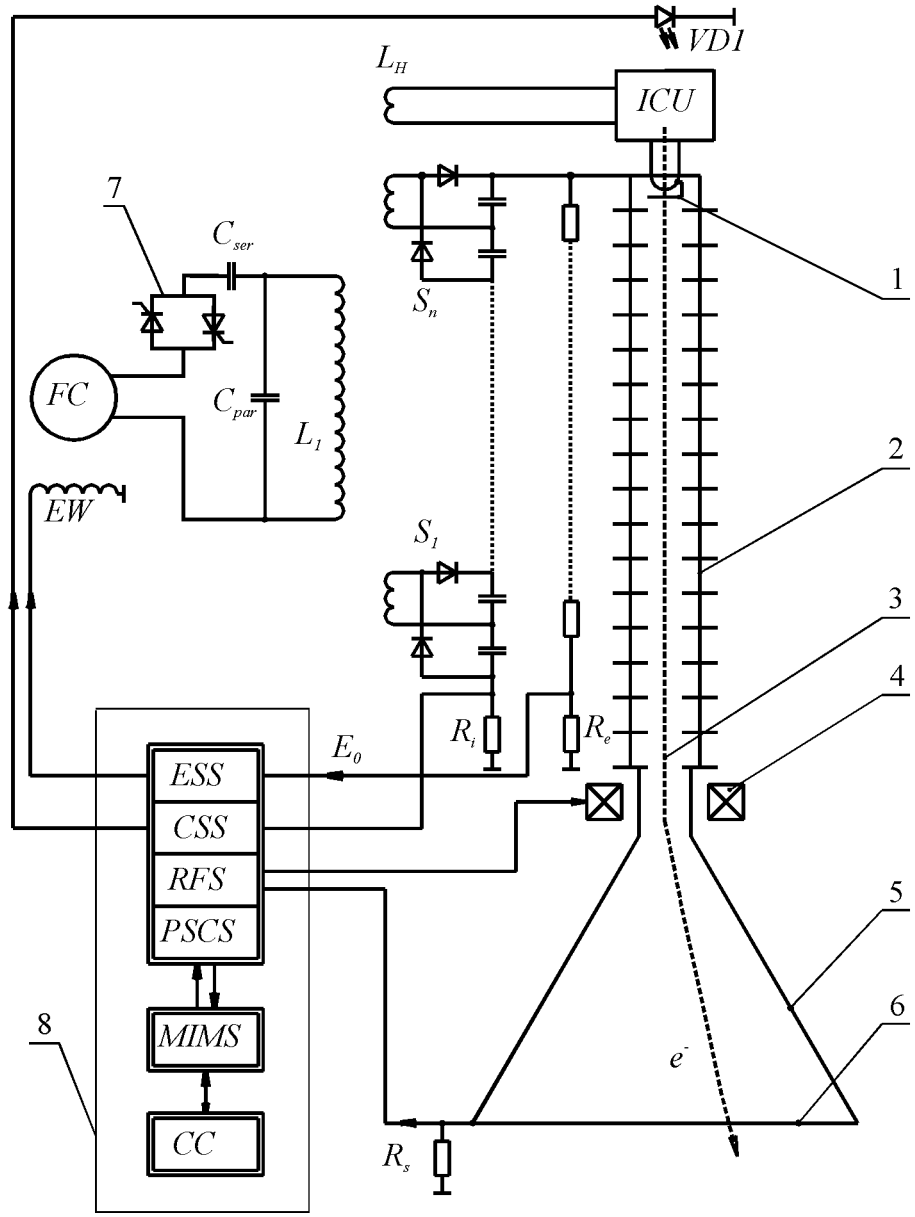

Figure 15. Simplified electric circuit of ELV accelerator. 1 — cathode of electron gun; 2 — accelerating tube; 3 — electron beam; 4 — coils of the raster formation system; 5 — extraction device; 6 — titanium foil; 7 — thyristor switch; 8 — control system (ESS — energy stabilizing system, CSS — current stabilizing system, RFS — raster formation system, MIMS — module information-measuring system, CC — Control Computer, PSCS — power supply control system). FC — frequency converter, ICU — injector control unit.

5. The steady-state H^- ion source with a beam current of up to 40 mA.

For a tandem proton accelerator for neutron generation, intended reliably to work in hospitals, it is necessary to create a steady-state reliable source of negative hydrogen ions with a long operation lifetime. The source should permit to obtain a H^- ion beam with a relatively small emittance and with a steady-state ion current of some tens milliamperes, as appear, not more 40 *mA*.

To satisfy these requirements, outcoming from our and world experience, we have chosen a surface-plasma source (SPS) in a multicusp geometry with a cesiated spherical emitter of H^- ions (a converter). A schematic diagram of the ion source is shown in Fig.16. It consists of a gas-discharge chamber with an internal diameter of about 12 cm and height of about 8 *cm*. Samarium-cobalt magnetized rods surrounded the chamber are shown in Fig.16 schematically. They form a multicusp "magnetic" wall of the discharge chamber. The multicusp magnetic wall will be optimized to improve a discharge plasma confinement in the final ion source design.

Hydrogen will be injected to the chamber through thin channels in the H^- ion emitter, as it is shown in Fig. 16. The discharge plasma in the chamber will be produced by an electron flux with an energy of $30 \div 60$ *eV* from LaB_6 cathodes. One or two cathodes will be installed in the chamber through a cylindrical wall. The LaB_6 cathode with a diameter of an emitting surface of 18 *mm* permits to get the 15 *A* electron current with a cathode lifetime of not less 2000 hours and 30 *A* with a lifetime of 500 hours. The design and technology of such cathodes are developed in the Institute [23]. We suppose, that a $15 \div 30$ *A* electron current will be sufficient for an ionization of hydrogen in the chamber with the good magnetic walls. The Mo-emitter of H^- ions will have a negative potential of about 100 *V* relatively the chamber and will be bombarded by plasma hydrogen ions. Adsorbed hydrogen atoms will be knocked off and atomic fragments of dropping ions will be reflected from an emitter surface.

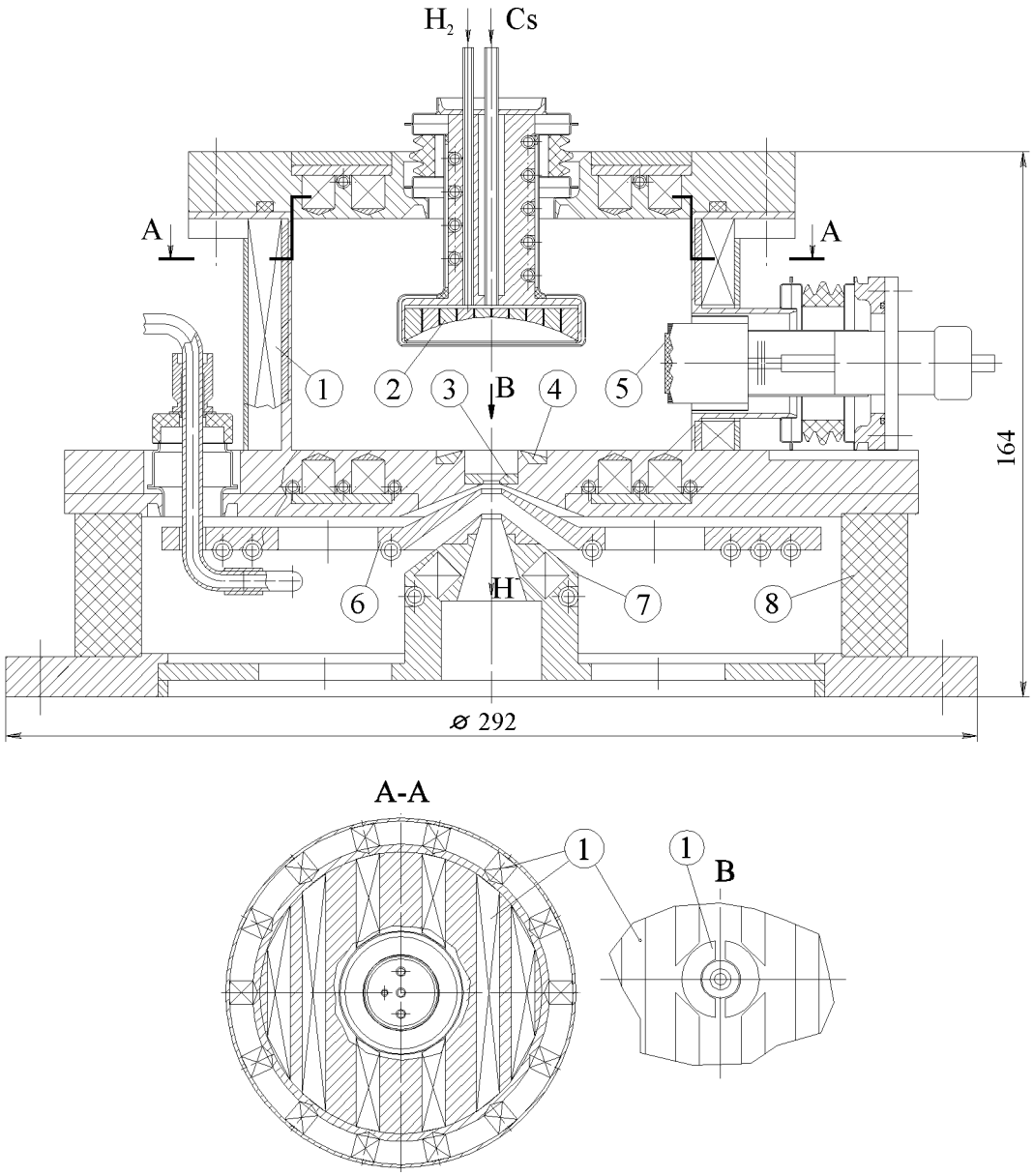

Figure 16. H^- ion source. 1 «magnetic» wall of gas discharge chamber, 2 emitter of H ions, 3 plasma electrode with outlet hole, 4 magnetic filter of electrons, 5 LaB_6 cathode, 6 extractor, 7 accelerating electrode, 8 30 kV main insulator.

A cesium vapor will come to the emitter surface through thin channels in it, as it is shown in Fig.16. Cesium will cover the emitter surface as owing to its diffusion on the surface, as a result of ionization of the cesium vapor injected from channels with a subsequent return of cesium ions by an electrical field to the surface. For the considerable reduction of the cesium condensation on the chamber walls, the hot thin metal shield will be used. A monolayer coverage on the H^- ion emitter surface will be produced at a cesium rate of few 1 *mg/h*. Thus a work function of the surface is reduced down to 1.5 *eV*. Due to the low work function fast

desorbed and reflected hydrogen atoms with an electron affinity of 0.75 *eV* leave the emitter surface as H^- ions with a probability close to an unity. The H^- ion emitter is a cold cathode with a high secondary ion-electron emission coefficient. The electron current from the emitter will be added to one from the hot LaB_6 cathodes. This can increase the ionization of hydrogen in the chamber. The H^- ions are accelerated by a near-electrode potential drop and are focused into an emission aperture on the anode wall of the chamber (3, Fig.16). Thus not all H^- ions left the emitter pass through the emission aperture.

Taken H^- emitter potential (about -100 V) allows us to convert hydrogen particles from plasma into H^- ions quite efficiently under significant limitation of cesium consumption [24-30].

On a basis of experience of work with SPS in a similar geometry developed in LBL [31], we expect that at a hydrogen pressure of not higher than 1 *mTorr* in the discharge chamber the stationary plasma with electron density of order 10^{12} cm^{-3} will be obtained. A minimum ion temperature is 0.1 *eV*. A hydrogen ion species ration of plasma depends on the hydrogen pressure and at the pressure of 1 *mTorr* ions are basically molecular (H_2^+, H_3^+) [32]. The appropriate current density of hydrogen atomic particles to the surface will be not less 0.1 A/cm^2, and the current to the 20 cm^2 emitter surface will be not less 2 *A*. Thus, about 400 *mA* of H^- ions will be emitted from the cesiated emitter surface [28,29,32].

The 100 *eV* H^- ions from the spherical emitter are focused into the emission aperture with a diameter of 0.5 *cm* on the anode. At distance from the emitter to emission aperture of 5 *cm* only H^- ions emitted with an mean angular spread of $\pm 2.5^o$ will pass the emission aperture. The mean angular spread of ions emitted from surface is approximately $\pm 5^o$. From here it follows that approximately 25 % of the H^- ion flux emitted from the converter pass through the emission aperture. At motion of H^- ions to the emission aperture they will be lost by gas and plasma. The main processes of H^- loss are:

$$H^- + H_2 \rightarrow H_0 + \dots ,$$

$$H^- + H^+, H_2^+, H_3^+ \rightarrow H_0 + \dots ,$$

$$H^- + e \rightarrow H_0 + 2e.$$

Because of the mentioned losses of H^- ions their flux from the emitter can be reduced by approximately 30 %. As a result about 18 % of emitted ions or about 70 mA can pass the emission aperture.

The H^- ion beam from the emission aperture will be accelerated up to 25 *keV* and move in hydrogen flowing from the emission aperture. Thus the initial mean free path of H^- ions because of their loss by hydrogen is 30 *cm*. With account of divergence of outflowing hydrogen $10 \div 15$ % of H^- ions will be lost. Based on it, according to estimations there is some reserve from the H^- ion current required.

For a formation and acceleration of the H^- ion beam the three electrode ion-optic system (IOS) is provided: a plasma electrode (3, Fig.16), an extractor (6) and accelerating electrode (7). The plasma and accelerating electrodes have Mo-insertions. According to a space charge of the emitted H^- ion beam with the current about of 50 *mA* the total gap in the IOS should be 9 *mm*. For reduction of an accompanying electron flux a magnetic filter (a local cross magnetic field over the emission aperture) is provided. In the IOS gaps a small counter cross magnetic field is formed, convex to the emission aperture. The electrons passed through the emission aperture are dumped along the convex magnetic field to the copper extractor. At allowable heating of a near beam edge of the copper electrode of up to 500° *C* it is possible to dump to it electrons with a power of up to 600 *W* (200 *mA* at extracting voltage 3 *kV*). In order to compensate the deflection of the H^- ions inside the electron magnetic filter, the position of the convertor will be corrected [33].

A vacuum chamber, through which the H^- ion source is connected to the tandem accelerator, is shown in Fig.17. The chamber is the two-volume cylindrical vacuum chamber with a diameter of 0.5 *m*, a total length of about 1 *m* and with a horizontal axis being in line with an axis of the tandem accelerating column.

The H^- ion source (1, Fig.17) is connected above to a cylindrical wall of the first volume (2) with the length of 0.6 *m*. The H^- ion beam enters the chamber from a top along a vertical, is turned 90° by a separating magnet, passes along a horizontal through a small aperture (9) in the wall into the second volume (3), intersects along the axis the second volume and is injected into the tandem accelerating column (14).

The H^- ion beam with the current 40 *mA* has a large enough space charge density and requires along a transport path from the ion source to the tandem accelerator a strong enough nearly continuous focusing. In front of the tandem entrance it is necessary to have a large spread of the beam with a minimum focus distance 5 *cm* from an initial point on a distance 11 *cm* from an external potential surface of the tandem accelerator. It is connected with a large force of an inlet lens formed by a field of the accelerator at the entrance. To satisfy to the mentioned conditions of injection of the ion beam into the tandem accelerator it is provided abruptly to focus the beam in the initial point (at 11 *cm* from the entrance) by pair of single electrostatic lenses (7,8) with a large aperture (maximal diameter of the beam in the lenses is $\approx 4 \div 5$ *cm*). This pair of the lenses ensures an ion-optical matching in the second volume, which is adjacent to the tandem accelerator.

The separating magnet (5) with two single electrostatic lenses installed before (4) and after (6) the magnet is located in the first volume. The H^- ion beam passes in the IOS the first 7 *cm* of the path in a compensated state, as far as in this area the density of gas, being flowing from the source, is high enough.

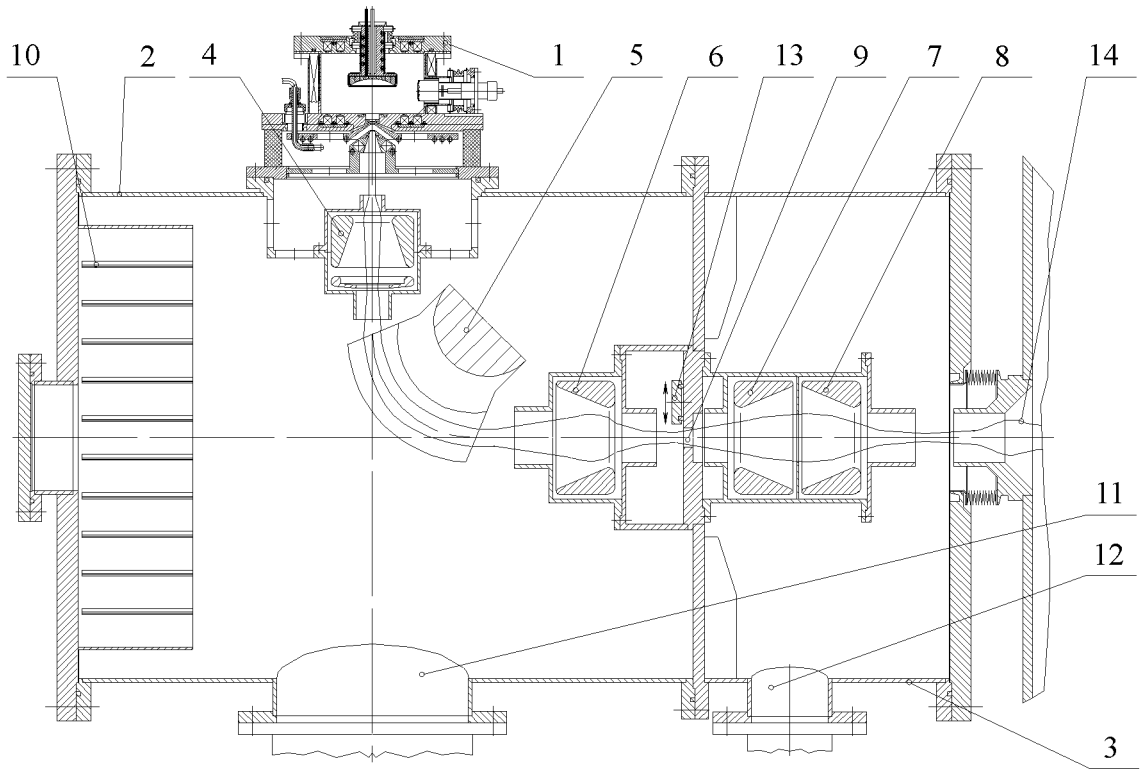

Figure 17. Chamber of H^- ion source. 1 H^- ion source, 2 1^{st} volume, 3 2^{nd} volume, 4, 6, 7, 8 electrostatic lenses, 5 separating (bending) magnet, 9 inter volume aperture, 10 shelves with zirconium powder, 11, 12 holes for turbomolecular pumps, 13 vacuum valve, 14 entrance into tandem accelerator.

At inlet into the first single lens the beam is decompensated and further is accompanied focusing by single lenses and the separating (bending) magnet. At the entrance into the second volume the beam is compressed in a diameter of down to $1.5 \div 2$ *cm*. It passes through the 2 *cm*-in-diam aperture in a diaphragm between the volumes.

At the 1 *mTorr* hydrogen pressure in the source through the emission aperture with diameter of 5 *mm* the hydrogen flow of about 10^{-2} *l Torr* s^{-1} enters the first volume. For maintenance of vacuum in the first volume with the pressure of 10^{-5} *Torr*, the pumping rate of 1000 *l/s* is necessary. Below the first volume a hole (11) with a diameter of 200 *mm* for connecting a 1000 *l/s* turbo-molecular pump is stipulated. The hydrogen flow 10^{-3} *l Torr* s^{-1} is injected into the second volume through the aperture in the diaphragm. A hole (12) with a diameter of 100 *mm* for connecting a 550 *l/s* turbo-molecular pump is stipulated below the second volume. The pumping of the second volume by this pump allows to maintain here vacuum of 10^{-6} *Torr*.

From the H^- ion source a cesium will be injected into the first volume in a quantity of a few *mg/hour* or $5 \div 10$ *g/year* at daily operation during 10 hours. For absorption of a cesium in the first volume on special shelves (10) a zirconium powder with grains of diameter 0.1 μm is located [34]. Zirconium has a high adsorption energy for Cs atom: 3.22 *eV* for a zero coverage and 2.55 *eV* for a monolayer. One litre of the powder at the monolayer Cs coverage of grains can absorb more than 15 *g* of cesium. Thus it is enough to place into the first volume 0.5 *l* ($\approx$ 2 *kg*) of the powder to ensure the absorption of cesium during one year of the operation approximately. A replacement of the powder can be made for some hours. The pressure of saturated cesium vapors for the Cs monolayer on zirconium is formally equal to zero. Therefore it is important only to prevent a direct hit of Cs atoms from the first volume to the second volume through the aperture in the diaphragm.

Another way of removal of a cesium is to establish a freon refrigerator and to cool special plates down to -30° *C* [35]. Thus the pressure of saturated cesium vapors in the first volume will not exceed 10^{-9} *Torr*.

We note that surface-plasma sources with using cesium operate many years on largest accelerators of the world. So magnetron-type SPSs operate from 1977 on accelerators in laboratories of FNAL, BNL, ANL, DESY, Ratherford Lab [36]. In majority of cases they were installed on Cockroft-Walter preinjectors with a stationary voltage of 750 *kV*. No influence of

cesium from SPS on an electric strength of accelerators was observed. The offered multicusp type of SPS is similar to one used many years on accelerators in laboratories of LANL [37] and KEK [38]. In LANL such a source operates from 1985 with a small duty factor: at the nominal current in a pulse of 20 *mA* the mean H^- ion current is 2 *mA*.

The separating magnet with a gap between poles of 3 *cm* is designed with the use of samarium-cobalt insertions. For the beam energy of 25 *keV* the product of the field by the turn radius is about 23 *kGs cm*. The turn radius is 12 *cm*. The appropriate magnetic field on the transport path is 1.91 *kGs*. The magnetic field of the samarium-cobalt magnet is varied 3×10^{-4} at a 1^{o} temperature variation. Since the turn angle should be kept accurate to within 10^{-3}, the magnet temperature should be stabilized by a cooling water with variation of its temperature within $\pm 3^{o}$. On the diaphragm between the first and second volumes a small vacuum valve (13, Fig.17) is provided which can close hermetically the aperture with a diameter of 2 *cm*. Due to this, not leaking the atmosphere in the tandem accelerator, one can leak the atmosphere in the first volume and to make a replace of the source cathodes, a replace of the zirconium powder and a preventive maintenance of the ion source and ion-optic elements. It should be emphasized that the only dry air should be leaked in the first volume to avoid a CsOH formation on walls. A harmless Cs_2O is formed at the leak-in of the dry air. A periodic leak-in of the dry air permits "to destroy" a metallic cesium in the vacuum chamber. Afterwards the atmosphere leak-in 3-5 hours is required for conditioning of the H^- ion source. If the source cathodes will have a operation lifetime of 2000 hours, this operation has to conduct 2 times per annum.

6. Neutron generating lithium targets

This project envisages a possibility of operation in two regimes of neutron generation - obtaining fast neutrons at an energy of a proton beam of 2.5 *MeV* during the formation of the necessary neutron spectrum with the use of the attenuator and the operation near the threshold of reaction ^{7}Li(*p*,*n*)^{7}Be at the proton energy of 1.885 *MeV* providing the generation of directed beam of neutrons with quite narrow spectrum at medium energy of ~ 30 *keV*. Therefore, it is desirable that the target design could be applicable to both these versions.

Since at the of 2 *MeV* the protons range in lithium is ~ 0.3 *mm* the target can be made in the form of the hard well cooled and placed into vacuum plate one side of which facing to the incident beam is coated by a thin layer of lithium which is the target. If the lithium moistens well the sublayer material, its thickness will be of a few tenths fraction of a millimeter and such a target can operate at temperatures above the lithium melting. The limit of target temperature will be the pressure of saturating lithium vapors increasing fast with temperature (Table 6). Dependence of lithium evaporation rate V_{ev} on temperature is also shown in Table 6.

Table 6.

T, °*C*	180	204	234	268	306	350	390	450	520
P_{sat}, *Torr*	10^{10}	10^{9}	10^{8}	10^{7}	10^{6}	10^{5}	10^{4}	10^{3}	10^{2}
V_{ev}, *g/cm²hour*	$3.4\cdot10^{9}$	$3.4\cdot10^{8}$	$3.4\cdot10^{7}$	$3.4\cdot10^{6}$	$3.4\cdot10^{5}$	$3.4\cdot10^{4}$	$3.4\cdot10^{3}$	0.034	0.34

Therefore, the operation at temperature above 400°*C* is undesirable since it leads to complications in pumping and to large consumption of, lithium. The target design is given in Fig.18.

It is a tungsten disk (1) in the form of a "plate" with 2 *mm* thick bottom. The inner surface of the "plate" is covered (moistened) by a thin layer of lithium (2). On the outer side of the "plate" the rectangular grooves 1 *mm* deep and 3 *mm* wide (3) covered by a 0.1 *mm* thick molybdenum foil (4). The foil is welded to the tungsten disk by the diffusional welding so that in the target bottom the narrow channels are made for cooling. On the end of each channel, there are round holes (5) connecting them to the collector cavities (6) made in the form of

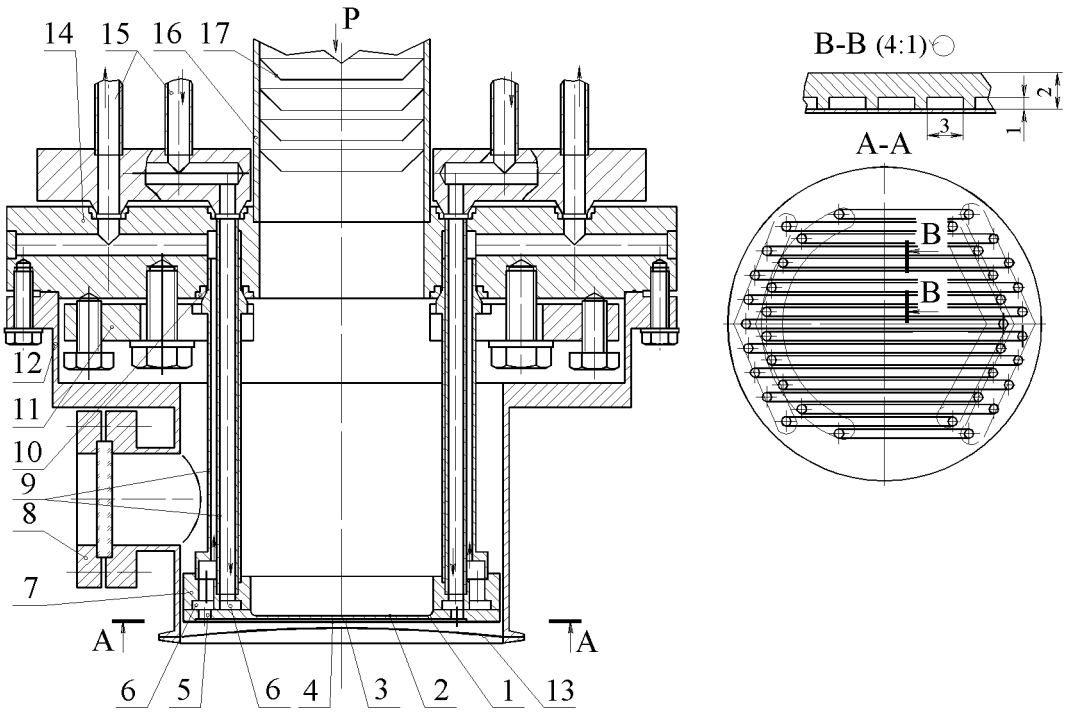

Figure 18. Neutron generating lithium target . 1 - tungsten disk; 2 lithium layer; 3 - cooling channels; 4 - tantalum foil; 5 - feeding holes; 6 - collector cavities; 7 - tantalum ring; 8 - observing window; 9 - feeding coaxial tubes; 10 - copper packings; 11 - lever clamps; 12 - vacuum chamber; 13 - molybdenum foil; 14 - body; 15 - heat carrier feeding tubes; 16 - vacuum chamber; 17 - cone caters of lithium vapors.

concentric half-rings in the thick tantalum ring (7) also welded to the tungsten by the diffusional welding.

Each narrow channel is connected in turn either from the inner or outer collector cavity that enables the passage of cooling liquid along the neighboring channels in opposite directions. The cooling liquid is applied to the opposite sides of the target disk through the pair of coaxial tubes (9) of which the outer tube is welded to the collector ring and the inner one is just tightly inserted into the outer tube. The feeding tubes are connected with the copper packings (10) to the collecting disk. The packing is provided by two lever clamps (11) so that the target can easily be connected to the body (14) after coating by lithium and testing on the special vacuum stand. After connecting the target it is covered by vacuum chamber (12) closed on the end by a thin molybdenum foil (13). The chamber has a view glass window (8) on its side cylindrical surface for the observation of the condition of lithium surface and electric inputs (not shown in Fig.) for the connection of thermal pairs measuring the temperature of the inner (lithium) and the outer surfaces of the target. From above, to the body the long vacuum

tube (16) is connected through which the pumping and drop of the proton beam onto the target is performed. On the inner surface of vacuum tube, the system of cone diaphragm-catchers of molecules of evaporating lithium (17). The cooling liquid is supplied to the target device through the feeding tubes (15), connecting it to the pump and heat exchangers.

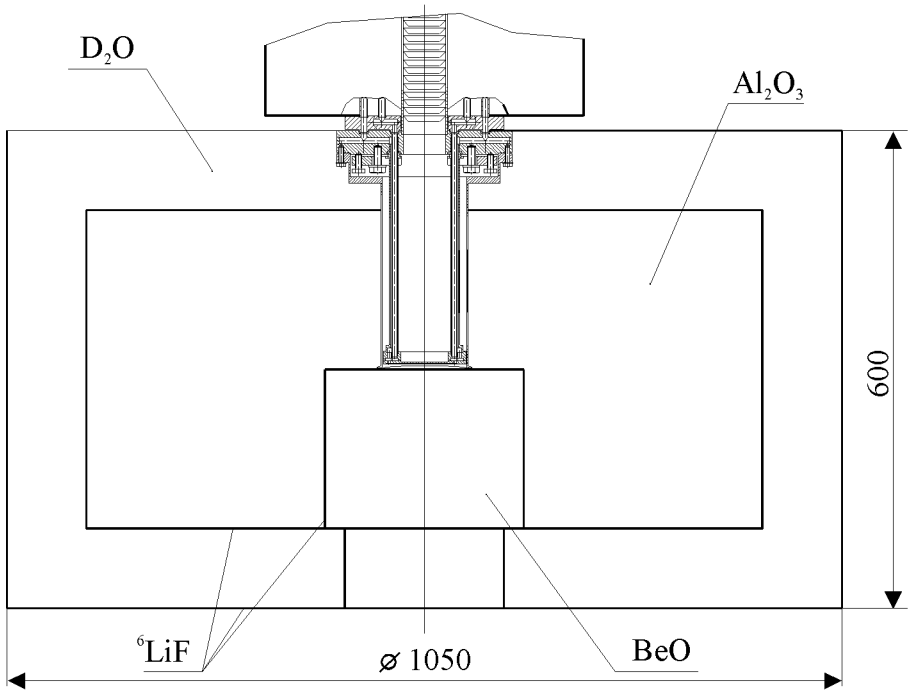

Figure 19. Target with moderator and reflector.

Thermal regime of target

The neutron generating target will be operated in the very complicated thermal regimes. At the proton energy of 2 MeV and an average beam current of 10 mA the power produced on the target surface will be $Q = 20\ kW$. At a beam diameter of 5 cm, the cooling made through the thin tungsten layer, should provide the evacuation of heat flux with density $q = 1\ kW/cm^2$.

The considered design enables the cooling of the target by any cooling liquid. Let us compare the cooling efficiency by water and by liquid metals — Gallium ($T_m \approx 30°C$) and mercury. If the temperature distribution over the lithium thickness $d_{Li} \approx 0.3\ mm$ is assumed to

be homogeneous (absorbtion length of 2 MeV protons in lithium is ~ 0.3 mm), its average temperature can be evaluated as: $T_{Li} \approx \Delta T_w + \Delta T_{w\text{-}liq} + T_{liq}$, where ΔT_w is the temperature drop on the tungsten wall, $\Delta T_{w\text{-}liq} = T_w - T_{liq}$ is the difference of temperatures of the cooling tungsten wall and liquid; T_{liq} is the temperature of cooling liquid. The temperature drop on tungsten can be estimated as: $\Delta T_w = q \cdot d_w / \lambda_w$, where d_w is the tungsten wall thickness, λ_w is the tungsten heat conductivity. The tungsten has the best among metals (except for silver, copper, gold) heat conductivity $\lambda_w \cong 1.3\ W\,cm^{-2}\,degree^{-1}$ within the temperature range $20 \div 300°C$. At $q = 1\ kW/cm^2$ and $d_w = 1\ mm$, $\Delta T_w = 80°$ and it is independent of the kind of cooling liquid. The heating of liquid upon its passage of cooling channel will be determined by its rate of flow $P = S \cdot V$ (S is the channel cross-section, V - liquid velocity) and by the thermal capacity. At our geometry ($S = 3 \times 1\ mm^2$) at the velocity of $V = 10\ m/s$ the rate of flow will be $P = 30\ cm^3/s$ and the maximum output temperature $T = q / C_p \cdot \gamma \cdot P$, where γ is the density, C_p is a mass thermal capacity (water $C_p = 4.2\ J\,g^{-1}degree^{-1}$; gallium $C_p = 0.37\ J\,g^{-1}degree^{-1}$, $\gamma_{Ga} = 6\ g/cm^3$; mercury $C_p = 0.14\ J\,g^{-1}degree^{-1}$, $\gamma_{Hg} = 13.6\ g/cm^3$). The liquid heating is: H_2O — $T_{liq} = 16°$, Ga — $T_{liq} = 30°$, Hg — $T_{liq} = 35°$.

The more complicated thermodynamic process determine the temperature drop between the cooled wall and heat carrier which at the convective heat exchange is expressed as $\Delta T_{w\text{-}liq} = q/\alpha$, where α — is the heat transfer factor which is determined by the hydrodynamic regime of liquid flow and by its thermodynamic properties.

For the effective cooling one has to provide the turbulent flow of liquid when the Reynold's number $Re = V \cdot d_r / \nu$ exceeds the critical value $Re > Re_{cr} = 2300$. Here V is the liquid velocity, ν (m^2/s) — kinematics factor of liquid viscosity and d_r is the characteristic transverse size of the channel. With the rectangular channel, $d_r = 4S/\Pi$, S is the channel cross-section area, Π is its circumference (in our geometry, $d_r = 1.5\ mm$).

The heat transfer coefficient is defined as $\alpha = Nu \cdot \lambda / d_r$. Here Nu is the Nusselt criterion defined by the empirical expression (critical equation): $Nu \approx 0.023\ Re^{0.8} Pr^{0.4}$, $Pr = \nu \cdot c_p \cdot \gamma / \lambda$ is the Prandtl criterion. For the liquid-metal heat carriers (Prandtl criterion $Pr >> 1$) by computing the efficient value of the Nusselt criterion one has to introduce the correction presented in terms of Peckle criterion [39] as $Pe = Re \cdot Pr$: $Nu_{eff} = Nu + 0.044 Pe^{0.75}$.

Table 7.

	γ, kg/m^3	λ, $W/m \cdot degree$	C_p, $J/kg \cdot degree$	ν, m^2/s
H_2O	10^3	0.65	$4.2 \cdot 10^3$	$1 \cdot 10^{-6}$ (20°C) $0.47 \cdot 10^{-6}$ (60°C) $0.2 \cdot 10^{-6}$ (100°C)
Ga	$6 \cdot 10^3$	27	$0.37 \cdot 10^3$	$0.2 \cdot 10^{-6}$
Hg	$13.6 \cdot 10^3$	9.5 (100°C))	$0.14 \cdot 10^3$	$0.1 \cdot 10^{-6}$ (100°C)

The main values determined the values of criteria *Re*, *Pr* and *Pe* are given in Table 7.

For water, the Prandtl criterion is much larger than that for metals and it strongly depends on temperature:

H_2O — $T = 20°C$ — $Pr = 7$; $T = 60°C$ — $Pr = 3.1$;

Ga — $Pr = 0.016$; Hg — $Pr = 0.016$.

The heat transfer coefficient α is strongly dependent on the heat carrier velocity V ($Re \sim V$). The choice of V is determined by the accessible consumption of the heat carrier and by the hydrodynamic pressure drop when flowing through the channel which is defined as follows:

$$\Delta P = \alpha \frac{l_k}{d_r} \cdot \frac{V^2}{2g} \gamma$$

($\alpha = 0.025$ for water). For water in our geometry at the velocity $V = 10$ *m/s*, P ≈ 0.5 kg/cm^2, so that higher velocities $V > 10$ *m/s* can also be considered. Table 8 shoes the computation results for $T_{w\text{-}liq}$ at $q = 1$ kW/cm^2 for various heat carriers at different velocities and the heat carrier temperature and pressure drop respectively when its flowing through the cooling channel.

It is seen that with water cooling the main contribution into the lithium layer temperature $T_{Li} \approx \Delta T_w + \Delta T_{w\text{-}liq} + T_{liq}$, is provided by the temperature drop between the cooling surface and heat carrier. Even at water velocity of 15 ÷ 20 *m/s*, in practice, T_{Li} reaches the melting temperature T_m=186°C. With an account for the non-uniform distribution of beam density and temperature drop over the lithium depth its surface will apparently be melted. An increase in water rate over 20 *m/s* is ineffective because of nonlinear dependence of $\Delta T_{w\text{-}liq}$ on V. Thus, the water cooling seems to be satisfactory at the proton beam current value not

exceeding 10 mA (q = 1 kW/cm^2). In the case of current increase up to 20 ÷ 40 mA, one has to shift to the liquid metal heat carriers. In this case, the cooling of tungsten surface will not be limited by temperature drop between its surface and cooling liquid $\Delta T_{w\text{-}liq}$ but the temperature drop over its thickness $\Delta T_w \sim q$ (at d_w = 1 mm, q = 1 kW/cm^2, ΔT_w = 80°) will be the limiting factor. Therefore, it is desirable to decrease tungsten surface thickness up to fractions of millimeter. At the operation with melted lithium at temperature $T_{Li} \leq 350$ C in the geometry under consideration, one can provide the cooling of the target by gallium up to current values of 40 mA.

Table 8.

	V, m/s	1	5	10	15	20
H_2O	P, kg/cm^2		0.15	0.6	1.3	2.3
	$\Delta T_{w\text{-}liq}$, °	600	270	160	110	90
	T_{liq} , ° C	160	32	16	11	
Ga	P, kg/cm^2	0.04	0.9	3.5	7.8	
	$\Delta T_{w\text{-}liq}$, °	60	46	35	29	
	T_{liq} , ° C	300	60	30	20	
Hg	P, kg/cm^2	0.08	2	8		
	$\Delta T_{w\text{-}liq}$, °	60	48	37	8	
	T_{liq} , ° C	350	70	35	23	

Such mode of work with the increasing of heat flux density to q = 4 kW/cm^2, probably, should be considered as hard feasible. As a reserve a compromise variant with the increasing of targets surface up 10 cm in diameter with corresponding decreasing of q may be considered. However it results in decreasing of neutron flux density — especially undesirable in works in the near threshold region without external collimator. Also it is necessary to bear in mind that with current of proton beam 40 mA full power releasing in the target will reach 100 kW — it essentially complicate the liquid lithium heat carrier pumping system and heat exchanger.

It was proposed in previous consideration that all the power of proton beam is released in the infinitely thin lithium layer. With finite thickness of lithium layer d_{Li} and uniform distribution of releasing power the temperature drop on lithium will be $\Delta T_{Li} = q \cdot d_{Li}/2 \cdot \lambda_{Li}$. Heat

conductivity of lithium is significantly less than the tungsten one $\lambda_{Li} = 0.53\ W\,cm^{-2}degree^{-1}$, so that with $q = 1\ kW/cm^2$ and thickness of lithium layer $d_{Li} = 0.3\ mm$ — the absorption length of 2.5 MeV protons, — the temperature drop will be $\Delta T_{Li} = 28°$. If the thickness of lithium layer is more than protons path then the temperature drop on additional lithium layer will be $\Delta T_{Li} = q \cdot d_{Li} / \lambda_{Li}$ and with full thickness, for example, $d_{Li} = 1\ mm$ will be $\Delta T_{Li} = 160°$. That's why desire to minimize the thickness of target up to $d_{Li} \le 0.1\ mm$, thickness where the effective neutron generation process have place, is caused only by requirements of heat removal.

Creation of such liquid lithium target and control of its thickness during long operation in conditions of evaporation will be one of technologically complicated problem during designing of target.

It is proposed to get thin lithium layers on the surface of tungsten disk by means of evaporation. A variant of special lithium vaporizer situated directly in target device (not shown at Fig. 18) and realizing evaporation of lithium continuously (or periodically switched) on the surface of target during operation, is considered. Thereby, necessary thickness of liquid lithium layer will be kept and controlled, for example, by value of neutron-flux. If temperature of target exceeds $300°C$ then appears a problem of pumping out of lithium vapours and of periodical cleaning of vacuum-guide surface in target region from absorbed lithium.

For horizontal proton beam the other variant of liquid lithium target is considered — in form of flat jet, flowing through the narrow nozzle. Liquid lithium in this case is pumped through the heat exchanger. The thickness of such target is not very crucial and can be 1÷2 *mm*. Such target device seems more perspective because with temperature of liquid lithium ~ $200°C$ we will not have practically any problems of evaporation ($P_{sat}=10^{-8}$ when $T = 230°C$) and limits of power removal are defined only by power of pumping system and heat exchanger.

It should be noted that technical problems of pumping system and powerful heat exchanger design in this case are practically similar with ones in target device cooling by intermediate liquid metal heat carriers. There is a big experience at BINP in creation of liquid lithium pumping systems [40] and jet targets from gallium-indium alloy and liquid lead developed for applying in high energy physics for secondary particles beam generation [41,42].

7. Conclusion

A project of proton accelerator complex for fast neutron therapy and for neutron-capture therapy is proposed and discussed in details.

This project is based on the experience accumulated at BINP in following directions.

1. The project of electrostatic accelerator tandem without accelerator columns — integral part of generally accepted accelerator scheme, is developed. Specifics of geometry of accelerating electrodes and tandem optics allows to reach maximum reliability in conditions of acceleration of high current proton beams in continuous mode and allows to ensure optimum conditions of pumping out the charge exchange target region and to use the reliable gaseous target of continuous operation. Main constructive and technical decisions of tandem construction were tested on 1 *MeV* prototype which operates now in pulsed mode of H^- ion source and is used as an injector in a synchrotron.

2. It is proposed to use the sectional rectifier (a part of the industrial ELV-type accelerator developed at BINP and widely used for technological aims in Russia and abroad) as a powerful high voltage source. There is experience of rectifier voltage stabilization with accuracy of 0.1%.

3. Wide experience has been accumulated at BINP in design of negative ion sources of different types and a well-known school of specialists in this field has been formed. It allows to create H^- continuous ion source with current 40 *mA* in short time.

4. Creation of lithium neutron-producing targets with high (up to several kW/cm^2) power density is based on wide experience of BINP in producing cylindrical lenses with solid or liquid lithium and liquid metal targets applied in high energy physics for secondary particles beam generation.

There is a pool of experience in Physics Energy Institute in Obninsk in dealing with proton beams of considered range of parameters, and there is a 2 *MeV* electrostatic accelerator with 2 *mA* current in Obninsk. Experimental works on optimization of lithium targets parameters and neutron beam forming both in "open" geometry and using moderators and reflectors can be carried out with this accelerator.

All aforesaid assures that the proposed accelerator complex can be created and transferred for exploitation in clinic during $1.5 \div 2$ years.

References

1. G. L. Locher. Bilogical effects and therapeutic possibilities of neutrons. Am.J. Roentgengenol. **36** (1936) 1.
2. R. V. Dorn. Boron neutron capture therapy (BNCT): a radiation oncology perspective. Int. J. Radiation Oncology Biol. Phys., **28**, 5 (1994) 1189.
3. R. F. Barth, A. H. Soloway, R. G. Fairchild, R. M. Brugger. Boron neutron capture therapy for cancer: Realities and prospects. Cancer, **70** (1992) 2995.
4. G. A. Miller, N. E. Hertel, B. W. Wehring, J. L. Horton. Gadolinium Neutron capture therapy. Nucl. Thechnol., **103** (1993) 320.
5. Yu. S. Mardinsky, A. S. Sysoev, V. G. Andreeb, I. A. Gudilov. Vorlaufige neutronen eines reactors bei der Strahlen-und kombinationstherapie von patienten mit kehlkoptkarrionos. Strahlentherapie und onkologie, n. 3, 1991.
6. H. B. Liu, R. M. Brugger, D. D. Greenberg, D. C. Rorer, J. P. Hu, H. M. Hauptman. Enhancement of the epithermal neutron beam used for BNCT at the BMRR. Int. J. Radiation Oncology Biol. Phys., **28** (1994) 1149.
7. W. A. Neuman, J. L. Jones. Conceptual design of a medical reactor for neutron capture therapy. Nucl. Technol., **92** (1990) 77.
8. R. M. Brugger, J. A. Shih, H. B. Liu. An epithemal neutron beam for neutron capture therapy at the Missouri university research reacor. Nucl. Technol., **98** (1992) 322.
9. A. V. Bondarenko, V. M. Litiaev, Yu. V. Matveev, V. A. Pivovarov, N. A. Soloviev, A. S. Sysoev. Conceptual disign of an economic and safe low power reactor for neutron therapy. Preprint FEI-2449, Obninsk, 1995.
10. J. C. Yanch, X. L. Zhou, R. E. Shefer, R. E. Klinkowstein. Accelerator-based epithermal neutron beam design for neutron capture therapy. Medical Physics, **19** (1992) 709.
11. C. K. Wang, T. E. Blue, R. A. Gahbauer. A neutronic Study of an Accelerator-based neutron irradiation facility for boron neutron capture therapy. Nucl. Technol. **84** (1989) 93.
12. Proceeding of the First international Workshop on Accelerator-based neutron sources for BNCT, Sept 11-14 1994, Jackson, Wyoning, USA. CONF-940976, Vol. 1, Vol.2, 1994.
13. Fast neutron Physics, Ed. by T.B. Marion and J.L. Fowler. Interscience Pubb. Inc., 1960.
14. V. N. Kononov, E. D. Poletaev, B. D. Yurlov. Absolute yield and spectrum of neutrons from $^{7}Li(p,n)^{7}Be$ reaction. Atomnaya Energia, **43** (1977) 303 (In English: Sov. At. Energy. **43** (1977) 947).
15. MCNP-A General Monte Carlo n-particle transport code. Version 4A, Ed. by Breismeister, LA-12625-M, 1993.
16. V. N. Kononov, V. I. Regushevsky, N. A. Soloviev. Accelerator-based intence and directed neutron source for BNCT. Paper L-9 at 7 International Symp. On neutron capture therapy for cancer. Sept 4-7, 1996, Zurich; Preprint FEI-2546, Obninsk 1996.
17. H. Liskien, A. Paulsen. Neutron production cross section and energies for $^{7}Li(p,n)^{7}Be$ and $^{7}Li(p,n)^{7}Be^{*}$. Nuclear Data Tables. **15** (1975) 1.

18. D. A. Allen, T. D. Beynon. A design study far an accelerator based epithermal neutron beam for BNCT. Phys. Med. Biol., **40** (1995) 807.

19. Experimental Nuclear Physics. Vol. 1, Editor E.Segre, New York - London, 1953.

20. L. N. Rozanov. Vacuum technology. - Moscow: Vysshaja shcola, 1990 (In Russian).

21. A. A. Glazcov, G. L. Saksagansky. Vacuum of the Electro-Physical enviroments and complexs. - Moscow: Energoatomizdat, 1985 (In Russian).

22. Yu. I. Golubenko, M. E. Veis, N. K. Kuksanov *et al*. Accelerators of ELV-type: status, development, applications. Budker Institute of Nuclear Physics, Novosibirsk. Preprint 97-7 (1997).

23. G. Kuznetsov. High temperature cathodes for high current density. Nucl. Instrum. and Methods Research, **A340** (1994), 204.

24. Yu. I. Bel'chenko, G. I. Dimov and V. G. Dudnikov. Physical principles of the surface plasma method for producing beams of negative ions. Proc. Symp. on Production and Neutralization of Neg. Hydrogen Ions and Beams. Brookhaven 1977, BNL 50727, p. 79 (1977).

25. J. Los, E. A. Overbosch and J. van Wunnik. Positive and negative ionization by scattering from surface. Proc. of 2nd Intern. Symp. on Production and Neutralization of Neg. Hydrogen Ions and Beams. Brookhaven 1980, BNL 51304, p. 23 (1980).

26. K. W. Ehlers, K. N. Leung. Effects of cesium in the plasma of the surface conversion H source. AIP Conf. Proc. No. 111 (1984), 258.

27. G. S. Tompa, W. E. Carr and M. Seide. Cesium coverage an molybdenum due to cesium ion bombardment. Appl. Phys. Lett., **48** (1986) 1048.

28. M. Seidl, W. E. Carr, J. L. Lopes *et al*. Surface production of negative hydrogen ions by hydrogen and cesium ion bombardment. AIP Conf. Proc. No. 158 (1987), 432.

29. M. Seidl, H. L. Cui, J. D. Isenberg *et al*. Surface production of negative hydrogen ions. AIP Conf. Proc. No. 287 (1992), 25.

30. J. D. Isenberg, H. J. Kwon and M. Seidl. Surface production of H ions by backscattering of H^+ and H_2^+ ions in the 3 50 eV ion energy range. AIP Conf. Proc. No. 287 (1992), 38.

31. K. W. Ehlers and K. N. Leung. Characteristics of a self extraction negative ion source. Proc. of 2nd Intern. Symp. on Production and Neutralization of Neg. Hydrogen Ions and Beams. Brookhaven 1980, BNL 51304, p. 198 (1980).

32. K. N. Leung and K. W. Ehlers. H ion formation from a surface conversion type ion source. Ibid, p. 65.

33. B. Piosczyk and G. Dammertz. Continuous operated H surface plasma ion source. Rev. Sci. Instrum. **57** (1986) 840.

34. G. I. Dimov. The matching of SPS to an electrostatic negative ion accelerator. AIP Conf. Proc. No. 210 (1990), 651.

35. C. W. Schmidt and C. D. Curtis. An H ion source for accelerator use. Proc. Symp. on Production and Neutralization of Neg. Hydrogen Ions and Beams. Brookhaven 1977, BNL 50727, p. 123 (1977).

36. G. I. Dimov. Use of hydrogen negative ions in particle accelerators. Rev. Sci. Instrum. **67** (1996) 3393.

37. R. L. York and R. R. Stevens. Development of a multicusp H ion source for accelerator application. AIP Conf. Proc. No. 111 (1983), 410.

38. S. Fucumoro, Z. Igarachi, K. Ikegami *et al.* 40 MeV proton injection linac with H beam. Proc. XIII Intern. Conf. on High Energy Accelerators, Novosibirsk, 1986, **1** (1987) 293.

39. S. S. Kutateladze. Heat transfer and hydrodynamics resistance. Moscow. Energoatomizdat. 1990 (in Russian).

40. B. F. Bayanov, G. I. Silvestrov *et al.* Large cylindrical lens with solid and liquid lithium. Proc. of I Europen Particle Accelerator Conference, Rome, June 1 11, 1988, **1**, 265.

41. G. I. Silvestrov. Problems of intense secondary particle beams production. Proc. of XIII Intern. Conf. of High Energy Accelerator, Novosibirsk, August 7 11, 1987, **2**, 258.

42. G. I. Silvestrov. Liquid metal targets for intensive high energy physics beams. Proc. of Workshop on New Kinds of Positron Source for Linear Colliders. March 4 7, 1997, SLAC, Stanford University, Stanford, California 94309, p. 346.